Universitat de les Illes Balears

MASTER'S THESIS

EFFECT OF ACOUSTIC OSCILLATIONS ON NON-EQUILIBRIUM STATE OF MAGNETIC DOMAIN WALLS IN CUBIC Ni-Mn-Ga SINGLE CRYSTAL

Anxo Fernández González

Master's Degree in Physics

(Specialisation/Pathway *Master's Degree in Advanced Physics and applied Mathematics*)

Centre for Postgraduate Studies

Academic Year 2021-22

EFFECT OF ACOUSTIC OSCILLATIONS ON NON-EQUILIBRIUM STATE OF MAGNETIC DOMAIN WALLS IN CUBIC Ni-Mn-Ga SINGLE CRYSTAL

Anxo Fernández González

Master's Thesis

Centre for Postgraduate Studies

University of the Balearic Islands

Academic Year 2021-22

Key words:

NiMnGa ; Domain walls ; Hysteresis ; Magnetomechanical

Thesis Supervisor's Name Dr. Sergey Kustov Dolgov

Abstract

Hysteresis in ferroic materials is a manifestation of non-equlibrium states of domain walls (DW): DWs are trapped in local energy minima. Depending on the intrinsic parameters of the system (height of the energy barriers) and external factors like temperature, DWs can be "frozen" in these metastable states or relax towards global energy minimum. Thermal fluctuation magnetic aftereffect is a classic example of magnetic domain wall relaxation in ferromagnets. In the present work we argue that acoustic oscillations in a ferromagnet, after application of magnetic field, can athermally move magnetic domain walls into a more stable configuration. We use in experiments stoichiometric Ni_2MnGa single crystals from the classical family of Ni-Mn-Ga magnetic shape memory alloys. The absorption of ultrasound versus strain amplitude is studied after a series of step-like increases of polarizing magnetic field followed by its decrease in the reverse sequence. A new phenomenon observed in the present work is "triggering" of the motion of magnetic DWs, trapped in the metastable states after step-like variation of polarizing field, by acoustic oscillations in the non-linear range of magnetic DW motion. In an attempt to confirm the observed effect we also determine the coercive field of magnetization hysteresis through the measurements of the reversible Villari effect. We show that the width of the hysteresis decreases when the acoustic oscillations in the non-linear range of DW motion are applied to the sample. The reported effect is explained in terms of periodic stress anisotropy field induced by ultrasonic oscillations.

Resumen

La histéresis en materiales ferroicos es una manifestación de estados de no equilibrio de las paredes de dominio magnético (PDM): las PDM están atrapadas en mínimos locales de energía. Dependiendo de los parámetros intrínsecos del sistema (altura de las barreras energéticas) y factores externos como la temperatura, las PDM pueden estar 'congeladas' en estos estados metaestables o relajarse hacia mínimos globales de energía. La secuela magnética de fluctuación térmica es un ejemplo clásico de la relajación de las PDM en materiales ferromagnéticos. En el presente trabajo discutimos que las oscilaciones acústicas en un material ferromagnético, tras la aplicación de un campo magnético, pueden mover las PDM atérmicamente a una configuración más estable. En los experimentos usamos monocristales de Ni_2MnGa estequiométrico de la clásica familia de aleaciones magnéticas con memoria de forma de Ni-Mn-Ga. La absorción de ultrasonidos versus amplitud de deformación se estudia tras una serie de aumentos paso a paso del campo magnético polarizante seguida de una disminución con la secuencia inversa. Un nuevo fenómeno observado en este trabajo es la 'activación' del movimiento de las PDM, atrapadas en los estados metaestables tras la variación paso a paso del campo polarizante, a causa de oscilaciones acústicas en el rango no lineal del movimiento de las PDM. En un intento de confirmar el efecto observado, también determinamos el campo coercitivo de la histéresis magnética a través de medidas del efecto Villari reversible. Mostramos que la anchura de la histéresis disminuye cuando se le aplican a la muestra oscilaciones acústicas en el rango no lineal del movimiento de las PDM. Dicho efecto se explica a través del campo anisótropo de estrés periódico inducido por oscilaciones ultrasónicas.

Index

1. Introduction

1.1. Domain walls in ferroic materials

Ferroic and multiferroic materials are characterized by ordering of certain parameter (strain of the crystalline lattice in ferroelastics, magnetic moments in ferromagnetics, dipolar moments in ferroelectrics). The ordered state of ferroics is observed below a certain temperature, called the Curie temperature T_C. Below T_C, ferroics acquire spontaneous strain, magnetization or polarization. If the ordered state is formed without applied external fields (mechanical stress, magnetic field, electric field for ferroelastics, ferromagnetics and ferroelectrics respectively), the material consists of so-called mesoscopic domains where the spontaneous strain, magnetization or polarization is uniform. The orientation of the spontaneous strain, magnetization or polarization is different in different domains. Domains are separated by 2-dimensional defects called domain walls (DW). Without an applied external field domains have different orientations of the spontaneous ordering, minimizing the stray field of the ferroic. Therefore, the net strain, net magnetization or net polarization of the ferroic is zero. If the external field is applied, the material acquires net strain, net magnetization, or net polarization due to the preferential orientation of the domains under the applied field. The resulting net values of strain, magnetization, or polarization originate from the rearrangement of the domain structure. The rearrangement of domain structure (in particular, so-called switching [1] of net strain, polarization or magnetization) is behind all useful properties of ferroic materials. Therefore, studying the dynamics of DWs is of a prime practical and theoretical importance. Another feature driving the interest to DWs is their unusual properties, different from the properties of the bulk material. The most intriguing examples are superconductive twin boundaries in WO_3 [2], polar twins in non-polar oxide ferroelastics like CaTiO3 [3] and polar tweed in $LaAlO_3$ [4]. Designing of specific DW properties for their applications in devices is referred to as “domain wall engineering” [1].

Another fundamental feature of ferroics is related with the phenomenon of hysteresis in the response of the ferroic to applied periodic field. A trajectory along a hysteresis loop represents a sequence of metastable states of the DW system. The phenomenon of hysteresis has been a subject of intense theoretical and experimental research, which has

resulted, e.g., in a three-volume textbook by Bertotti and Mayergoyz [5]. The acoustic methods of studying the dynamics of magnetic DWs and of the magnetoelastic hysteresis are especially attractive: the stress-induced motion of magnetic DWs changes (locally and globally) the magnetic flux and creates a complex pattern of eddy currents. Eddy currents are responsible for dissipation of energy which can be conveniently detected. Acoustic methods are perfectly suited for studying magnetic DW dynamics due to a very wide spatial scale involved: from much less than magnetic domain width up to the characteristic sample dimension [6].

1.2. Magnetic domain walls and magnetomechanical damping

Magnetomechanical damping (MMD) is defined any damping suppressed by saturating magnetic field [7]. It includes contributions from magnetic DWs (microeddy and hysteretic terms) and macroeddy term that originates from the variations of macroscopic net magnetization of the sample.

Magnetic field interacts with magnetic DWs provoking net magnetization change and, therefore, can serve as an instrument for studying domain wall dynamics in ferromagnetics. However, relatively high-frequency periodic magnetic field does not penetrate into the volume of a ferromagnet, strongly limiting the use of the periodic magnetic field. On the other hand, periodic stress can be applied to the entire volume of a sample. Due to magnetoelastic coupling, the stress is equivalent to an effective magnetic field, which can be induced in the volume of the sample. For an isotropic ferromagnet with saturation magnetostriction λ_s, an applied mechanical stress σ induces a magnetoelastic energy per unit volume [8]:

$$W_{me} = \frac{3}{2}\lambda_s \sigma \sin^2\theta, \tag{1}$$

where θ is the angle between the magnetization and the stress directions. Due to the magnetoelastic energy (1), the applied mechanical stress acts on non-180° domain walls as an effective magnetic anisotropy field [8]:

$$H_\sigma \cong \frac{3}{2}\frac{\lambda_s \sigma}{\mu_0 M_s}, \tag{2}$$

where M_s is the saturation magnetization.

Thus, the periodic mechanical stress can be employed to efficiently induce the magnetic field in the interior of the sample, the motion of domain walls and this way to track their dynamics through the domain wall-induced absorption of energy. The domain wall - related absorption of mechanical oscillations is a part of the MMD. Another contributor to the MMD is variation of the net magnetization of the sample.

The components of MMD are [9,10]:

- a *linear* micro eddy current damping, δ_μ, measured at low strain amplitudes,
- a *linear* macro eddy current damping component, δ_M, and
- a *non-linear* hysteretic damping, $\delta_h(\varepsilon_0)$, emerging at higher strain amplitudes.

In the present context, linear damping δ_i is defined as being independent of the vibrational strain amplitude ε_0, the hysteretic damping component shows a significant increase with ε_0.

These components are associated with different length scales: δ_μ is commonly ascribed to short-range reversible domain wall displacements (much) less than the average dimensions of magnetic domains, δ_h is associated with larger-scale irreversible domain wall motions, more comparable with domain sizes. δ_M is measured at a scale comparable with the penetration depth of the macroscopic electromagnetic wave, averaging over many domains. Due to very different spatial scales involved in the linear and non-linear mechanisms of magnetomechanical damping, their contributions to the overall damping are additive, as is explained schematically in Fig. 1.

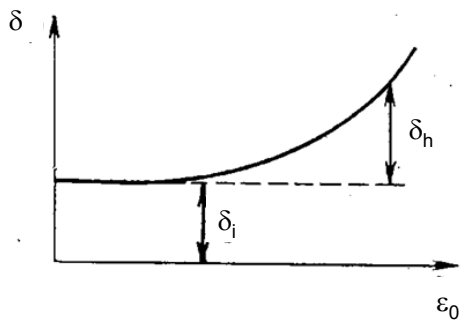

Figure 1. Schematic representation of the decomposition of the total damping δ measured as a function of strain amplitude ε_0 into the low-amplitude linear (strain amplitude independent) component δ_i and high-amplitude non-linear term δ_h (adapted from [9]).

All three MMD components depend on *H* and vanish at saturation. δ_i and $\delta_h(\varepsilon_0)$ display their maximum values either for zero magnetization $M = 0$, $H = 0$, or in its vicinity, then decline monotonously with applied field H [9,10]. δ_M has its maximum value at *H* slightly above half the saturating field; for $M = 0$, $\delta_M = 0$ [9,10]. Thus, studies of MMD components versus field and strain amplitude show aspects of the domain wall dynamics at various length scales. δ_μ shows a Debye type maximum at frequencies f at ca.10^5-10^6 Hz [11], and is usually negligibly small below 10^3 Hz and above 10^7 Hz. The macroeddy component is a superposition of a series of Debye relaxations. The most pronounced one is the fundamental component having the lowest frequency typically around 10^3 Hz. Both micro- and macroeddy current Debye relaxations are characterized, apart from the frequency, by a relaxation strength. Detailed analysis of the strength and frequency of eddy current relaxations is given in Ref. 11.

The non-linear hysteresis MMD component δ_h depends on strain amplitude ε_0 but not on frequency. It is supposed to originate from the long-range motion of domain walls through randomly distributed internal stress fields. The motion of domain walls across internal stress fields is responsible for stress-anelastic strain hysteresis. Smith and Birchak [12,13] postulated several specific hysteresis loop shapes that would obey the Rayleigh law at low strain amplitudes (their area should be proportional to the cube of the stress/strain amplitude $\Delta W \propto \sigma_0^3$). For an exponential distribution of stress fields

and low strain amplitudes (Rayleigh region) they obtained a solution for the hysteretic damping versus strain amplitude as:

$$\delta_h = K\frac{E^2\lambda}{\sigma_i^2}\varepsilon_0, \qquad (3)$$

where K is a numerical factor, E is the unrelaxed Young´s modulus at saturation, λ is the magnetostriction constant and σ_i is a certain measure of the internal stresses. The solution given by Eq. (3) follows the Rayleigh law which implies the linear dependence of hysteretic damping on strain amplitude.

1.3. Ni_2MnGa ferromagnetic shape memory alloy

Ni-Mn-Ga system of alloys is a typical representative of such multiferroic functional materials as ferromagnetic shape memory alloys. Main functionality of these alloys stems from the coexistence of ferroelasticity and ferromagnetism [14], resulting in large magnetic field induced strains on the order of 10%. Below the temperatures of ferroelastic and ferromagnetic ordering elastic and magnetic domains coexist. Ferromagnetic ordering in Ni-Mn-Ga is the second order transition, ferroelastic ordering is the first order structural transition in the solid state (referred to as martensitic transformation). To describe the martensitic transformation therefore one needs 4 characteristic temperatures: start and finish temperatures of the direct (martensitic) transformation on cooling (M_s and M_f) and start and finish temperatures of the reverse (austenitic) transformation on heating (A_s and A_f). Elastic domains are twins or so-called martensitic variants. Martensitic variants can be reoriented by applied magnetic field due to the high magnetocrystalline anisotropy in the low-temperature multiferroic state, resulting in high magnetic field induced strains [15].
Near stoichiometric Ni_2MnGa alloy has a complicated sequence of magnetic, premartensitic and martensitic transformations which can be revealed, for example, by real and imaginary components of the ac impedance. Figure 2 shows corresponding data taken from Ref. [16].

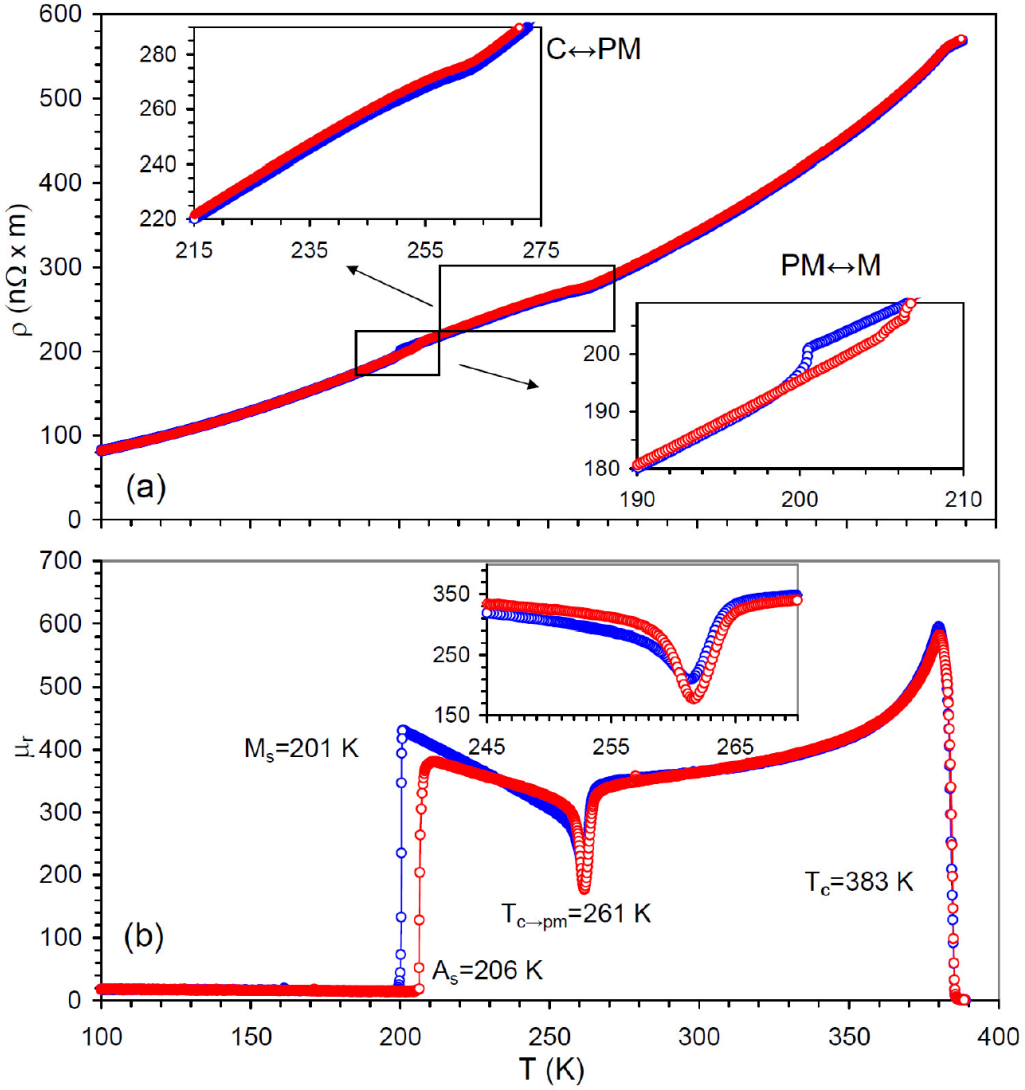

Figure 2. Temperature dependence of resistivity ρ (a) and relative permeability μ_r (b) for a Ni_2MnGa single crystal registered during cooling (blue symbols) and heating (red symbols). Characteristic temperatures of the phase transitions are shown in (b):

- **Curie temperature of the ferromagnetic ordering T_C=383 K**
- **Cubic-Premartensitic transition temperature on cooling $T_{c\rightarrow PM}$ =261 K**
- **Start temperatures of the direct M_s=201 K and reverse A_s=206 K martensitic transformations.**

The insets show details of the resistivity during Cubic-Premartensitic and Premartenstic-Martensitic transformations (a) and details of the permeability minimum during premartensitic transition (b). Extracted from Reference [16].

In the present work the same Ni_2MnGa single crystals were used as in Ref. 16 (data shown in Figure 2). According to Figure 2, the ferromagnetic ordering temperature (the Curie temperature T_C) is ca. 383 K, the start temperatures of the direct martenstic transformation on cooling M_s=201 K and of the reverse martensitic transformation on

heating A_s= 206 K. The temperature of the cubic-premartensitic phase transition on cooling is $T_{c\rightarrow PM}$ =261 K. The cubic-premartensitic structural transition is weakly first order and shows rather narrow temperature hysteresis between cooling and heating approximately 1 K, see e.g. inset in Figure 2(b).

There are several reasons for selecting ferromagnetic Ni_2MnGa crystals as objects for studying magnetic DW dynamics. First, the existence of magnetic DWs is often totally neglected in recent interpretations of magnetic and acoustic properties of different Ni-Mn-Ga crystals, see e.g. [17]. Second, the mobility of magnetic and twin boundaries is a key issue in applications of Ni-Mn-Ga alloys and is a subject of intense research [14,18]. Third, single crystals available at the group of Physics of Materials, UIB, are the best quality single crystals supplied by the Materials Physics Laboratory (MPL) of Lappeenranta-Lahti university of Technology. The group of Physics of Materials has a long-term collaboration with MPL and the crystals available are rather well characterized. Some relevant characteristics of the Ni_2MnGa crystals used in this work are presented in Figures 3 and 4.

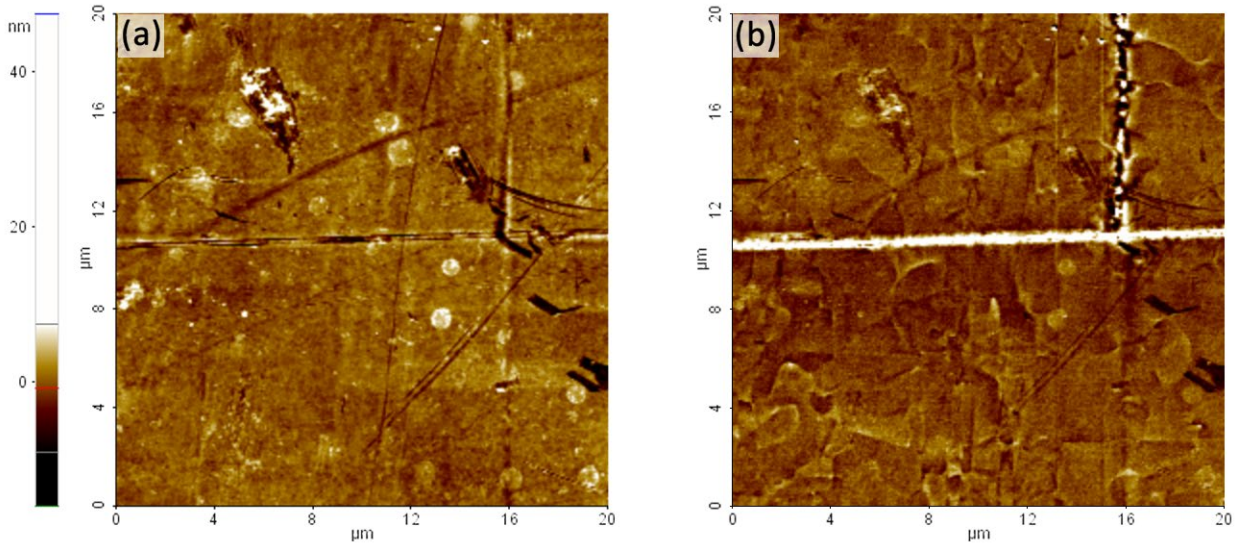

Figure 3. Atomic force Microscopy topography (a) and phase signal maps obtained by Magnetic Force Microscopy scan (b) of a sample of Ni_2MnGa single crystal. Surface orientation is of (100) type. Extracted from Reference [19].

Figure 3, taken from Reference 19, shows surface topography image (a) of a part of a Ni_2MnGa single crystal and magnetic DW structure (b) of the same area revealed by Magnetic Force Microscopy using phase signal contrast mode. Magnetic DWs have

irregular shape without any preferential crystallographic orientation due to very weak magnetic anisotropy of cubic Ni_2MnGa [20,21]. This legitimizes using simple fundamental relations (1,2) to estimate magnetoelastic properties of the Ni_2MnGa samples. The avearge size of the domains is rather small, between 1 and 10 micron. Figure 4 shows magnetization curves for a crystal similar to the one studied in the present work at temperatures 360 and 320 K, taken from Reference [19]. These data allow one to determine the saturation magnetization of the material over this temperature range as $\mu_0 M \approx (0.4\text{-}0.6)$ T.

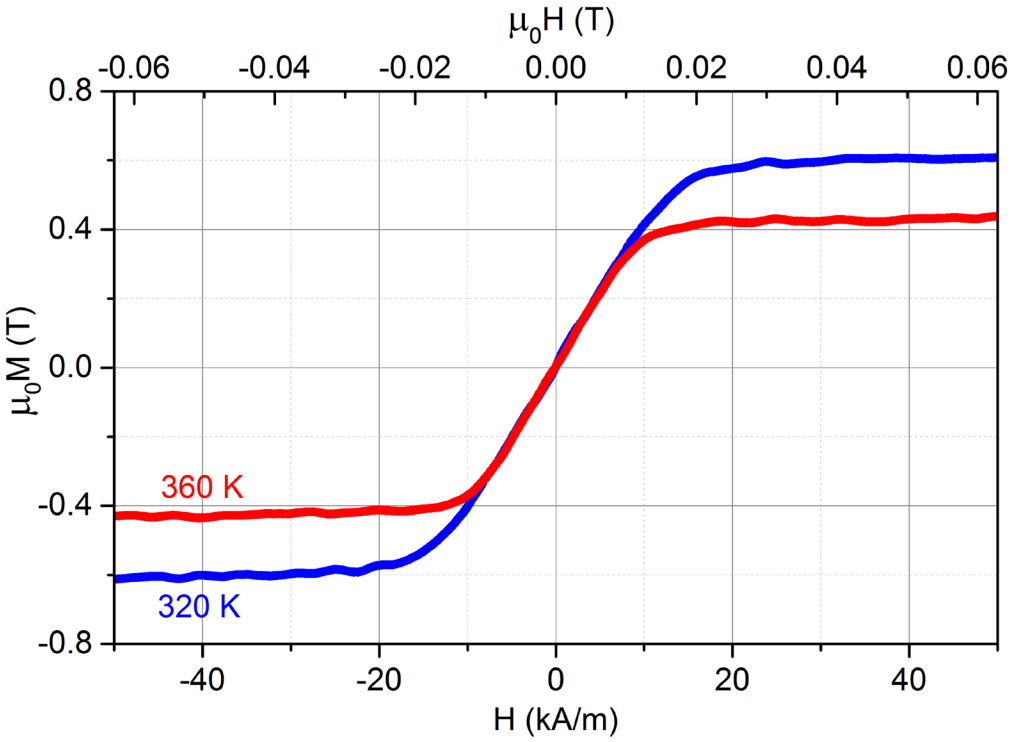

Figure 4. Magnetization curves for the Ni_2MnGa single crystalline [100] sample taken at 320 and 360 K. Extracted from Reference [19].

2. Material and experimental techniques

2.1. Piezoelectric composite oscillator technique

The acoustic measurements were performed using the Piezoelectric Ultrasonic Composite Oscillator Technique (PUCOT), described in detail in [22].
The method consists in inducing longitudinal resonant oscillations in the sample (bar) at a frequency around 100 kHz. The oscillations are induced by a quartz resonator that consists of the drive and gauge transducers, the unit consisting of the sample and the resonator is referred to as 'oscillator' (Figure 5).

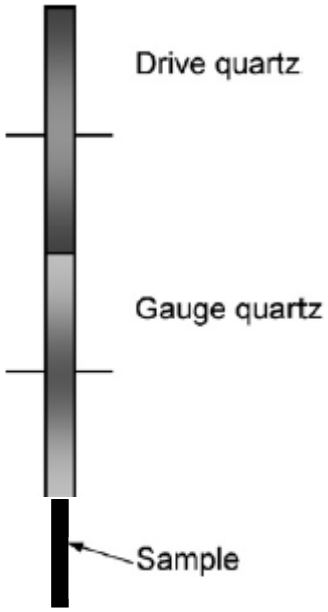

Figure 5. Schematic drawing of the ultrasonic oscillator consisting of two quartz transducers (Drive quartz and Gauge quartz) and a sample attached to the transducers.

Detailed theory of PUCOT has been developed by Robinson and Edgar [22]. The transducers of so-called 18.5º X-cut quartz use the transverse piezoeffect. The main parameters that are registered at resonance and determine the internal friction of the oscillator (expressed for instance as logarithmic decrement δ), strain amplitude ε_0 and Young´s modulus E are the two voltages across the transducers and the resonant frequency of the oscillator f. The ac voltage applied to the drive quartz, Ud, excites the oscillations. The voltage picked up across gauge quartz, Ug, serves to determine the strain amplitude. The most convenient and fast method is the creation of a positive

feedback loop from Ug to Ud which provides the amplitude and phase conditions for the resonance [23]. This method of measurements has been employed in the present work.

The solutions for the logarithmic decrement of the oscillator and oscillatory strain amplitude are [22]:

$$\delta = k_\delta \frac{U_d}{U_g} \tag{4}$$

$$\varepsilon_0 = k_\varepsilon U_g , \tag{5}$$

where k_δ and k_ε are numerical factors depending on the fundamental quartz constants and geometry of the transducers [22].

The damping and the resonant frequency of the sample δ_s and f_s, respectively, are derived from the corresponding parameters of the oscillator (that are measured in the experiment) and of the quartz transducer alone, δ_q and f_q:

$$\delta_s = \frac{\delta(m_s + m_q) - \delta_q m_q}{m_s} \tag{6}$$

$$f_s = \frac{f(m_s + m_q) - f_q m_q}{m_s} , \tag{7}$$

where m_s and m_q are the masses of the sample and quartz transducer alone, respectively.

The Young´s modulus E of a bar-shaped sample with length l and density ρ oscillating in the fundamental longitudinal mode is:

$$E = 4\rho f_s^2 l^2 . \tag{8}$$

Figure 6 shows a schematic block-diagram of the experimental setup for measurements of the internal friction and Young´s modulus of the samples of the samples at different temperatures by means of PUCOT. The PUCOT electronics block measures two ac

voltages, Ud and Ug, and generates the output signal that serves to maintain the phase and amplitude conditions of the self-oscillations. This signal is amplified by Krohn-Hite 7602 power amplifier with symmetric output that feeds the drive quartz. The maximum value of output voltage provided by Krohn-hite 7602M is 800 V root mean square value. With this voltage, the strain amplitude of the oscillations can reach approximately $2*10^{-4}$. The frequency of oscillations is measured by means of the digital frequency meter Agilent 53132, temperature in the vicinity of the sample is registered by means of the platinum resistor PT-100, connected to the multimeter HP 3478 A. All digital devices are connected to the personal computer PC by means of the GPIB bus. The oscillator with the sensor is placed inside the furnace, which in its turn is located inside liquid nitrogen cryostat. The temperature range of measurements is between 80 and 400 K.

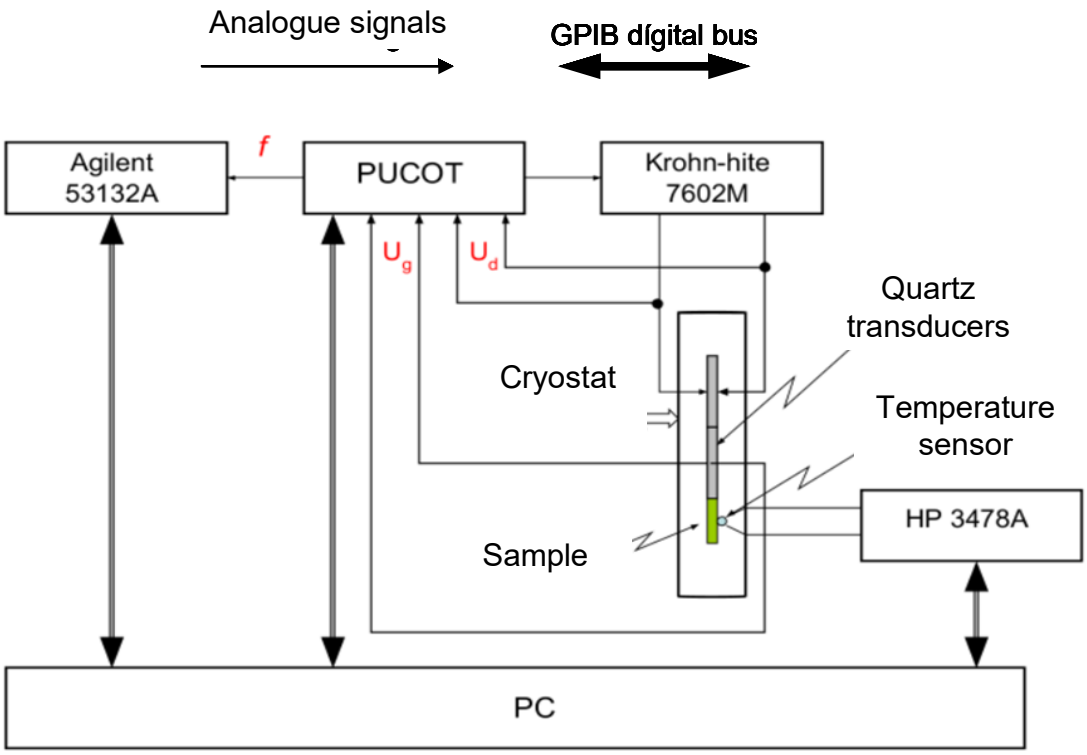

Figure 6. Schematic block diagram of the experimental setup for measurements of the internal friction and Young´s modulus of the samples.

PUCOT – block of the PUCOT electronics
Agilent 53132A – frequency meter
Krohn-hite 7602M – symmetrical output power amplifier
HP 3478 – digital multimeter
PC – control computer

The polarizing axial magnetic field is applied to the entire oscillator by means of a long solenoid (600 mm long) placed around the cryostat. The maximum value of the applied magnetic field is 18 kA/m, the non-uniformity of the field in the volume containing the sample is less than 0.5%.

2.2. Mechanomagnetic spectroscopy

The Mechanomagnetic Spectroscopy [24,25] is a modification of the PUCOT which allows one to measure the reversible inverse magnetostriction or Villari effect of magnetic materials simultaneously with the internal friction and Young´s modulus. The idea was to pickup the magnetization (magnetic flux density) periodic variations

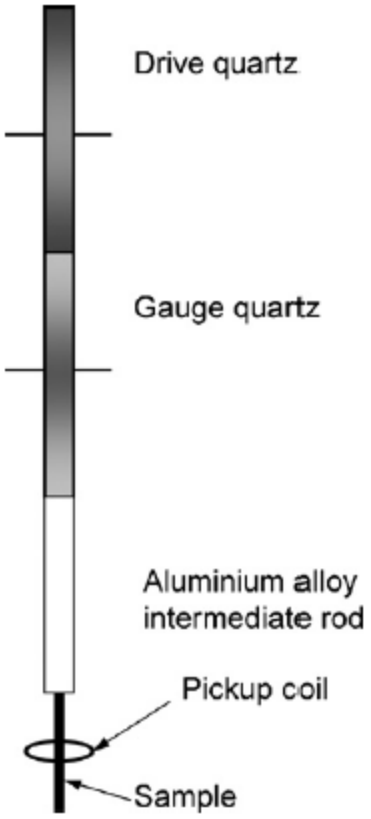

Figure 7. Schematic drawing of the PUCOT oscillator in the mechanomagnetic spectroscopy mode. After [25].

induced in a magnetic sample by periodic applied stress. The experimental realization consists in placing a small pickup coil around the middle section of the sample (stress and strain antinode for the fundamental standing wave mode). The schematic drawing

of the PUCOT modified for mechanomagnetic spectroscopy mode is shown in Figure 7 [25]. Apart from the pickup coil, in some cases (low values of magnetostriction), an additional intermediate resonant bar from non-magnetic low-damping material is added in between the sample and the quartz transducer. This bar serves to minimize the cross-talk between the signal in the coil and ac voltages across the transducers.
We can measure the flux density variations in the sample from the voltage in the pick up coil. The amplitude of the voltage V:

$$V = \left(\frac{d\Phi}{dt}\right)_{\max} = nS\omega B_0 \qquad (9)$$

where Φ is the magnetic flux penetrating the coil, n and S are the number of turns in the coil and the cross-section area of the sample, B_0 is the amplitude of stress-induced flux density and ω is the angular frequency of oscillations. The voltage induced in the pickup coil is measured by means of the lock-in amplifier in order to improve the signal/noise ratio. The lowest value of the voltage in the pickup coil is approximately 1 microvolt. This value of voltage for the conventional cross-section of the sample (1.5 * 1.5 mm2) corresponds to the amplitude of induced periodic magnetic flux approximately 1 nT.
Figure 8 is a photo of the oscillator with Ni_2MnGa sample placed inside the pickup coil. The signal was rather high in the case of Ni2MnGa sample and there was no need to use an intermediate non-magnetic bar between the quartz transducer and the sample.

2.3. Experimental protocols

First type of experiments

In the first experiment the sample was first thermally demagnetized by heating it above the Curie temperature (up to 388 K). Then the sample was cooled down to the desired temperature without applied magnetic field. After reaching and stabilization of the desired temperature, the strain amplitude dependence of the damping and resonant frequency was registered for the demagnetized state of the sample. After that, the polarizing magnetic field was applied to the sample in step-like manner with the step of

1.5 kA/m. After application of the field, two consecutive strain amplitude scans were performed.

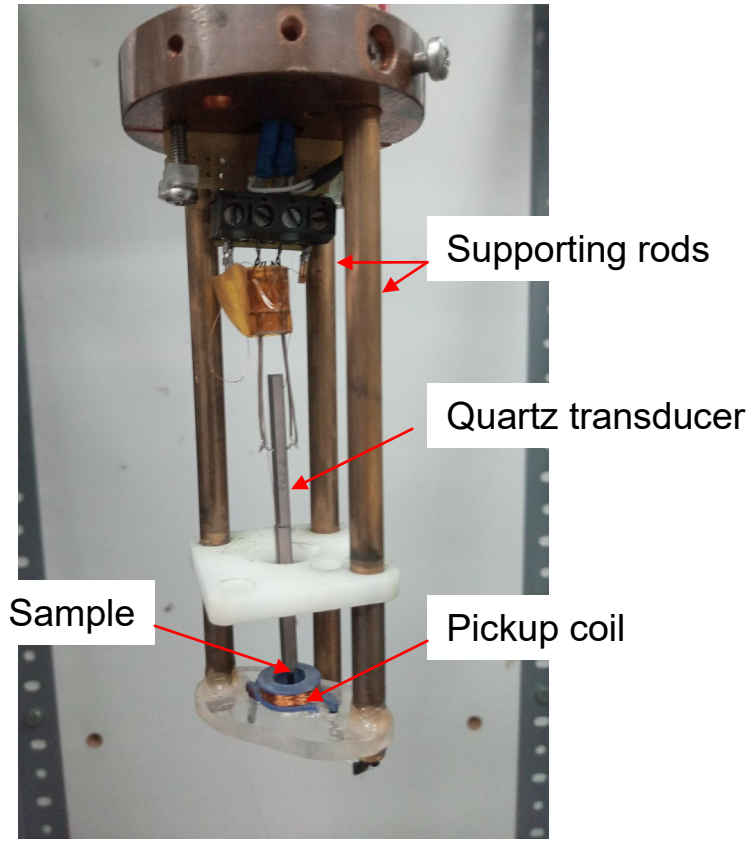

Figure 8. Experimental arrangement of the oscillator with the sample placed inside the pickup coil in the Mechanomagnetic Spectroscopy mode of the PUCOT. The idea of the spatial scale is given by the length of the two quartz transducers of 56 mm.

Second type of experiments

In the second type of experiments the PUCOT in the Mechanomagnetic Spectroscopy mode is used. That means that, in addition to the damping and resonant frequency, the reversible Villari effect (RVE) was simultaneously registered.

In these group of experiments the sample was again first thermally demagnetized. Then the RVE, internal friction and resonant frequency were registered on cooling to the desired temperature under constant value of oscillatory strain amplitude without polarizing field. In one of the experiments, the temperature spectra were registered under polarizing field and between 390 and 230 K, covering the range of the premartensitic transformation at T=260 K. After reaching and stabilization of the

desired temperature, the RVE, internal friction and resonant frequency of the oscillator were measured as a function of applied polarizing field. During the measurements the strain amplitude was kept constant at either a low value of $2*10^{-7}$ or at a high value of 10^{-5} . Two cycles of the saw-tooth magnetic field were applied in each experiment. The frequency of the cyclic magnetic field was 0.001 Hz (period of 1000 s).
100 experimental points were measured in each cycle of applied field. That means that each hysteresis loop consisted of 100 experimental points. The RVE hysteresis was studied in the cubic phase at T=343 K, T=303 K, and in the premartensitic phase at T=250 K.

2.4. Samples

Two single crystalline samples of nearly stoichiometric Ni_2MnGa were used in all experiments. The samples were provided by the Physics of Materials laboratory, Lappeenranta University of Technology (LUT) and were the same as used in experiments of Ref. [11]. The samples were oriented along [100] axis. Sample #1 had a length of 6.5 mm, Sample #2 – 11.2 mm, both of them had a cross section of 1.1 mm^2. Samples of different lengths were studied in order to cover a wider range of measuring temperatures: the Young´s modulus of Ni_2MnGa changes strongly and rapidly between the Curie and premartensitic transformation temperatures [11]. Therefore, the resonant frequency of the shorter sample #1 corresponded to the temperature range between the Curie and room temperature, whereas the longer sample #2 was optimized for the measurements between the room temperature and premartenitic transformation range. Samples were prepared at LUT: oriented, cut, annealed and chemically etched.

3. Experimental results

3.1. Strain amplitude hysteresis of the ultrasonic absorption under increasing and decreasing polarizing magnetic field

Figure 9 shows strain amplitude dependence (SAD) of the ultrasonic absorption in Ni_2MnGa sample #1 taken at 343 K. The elevated temperature was chosen in order to reduce the saturating field and thus to arrive rather close to the saturation under maximum available fields not exceeding ca. 18 kA/m. The sample was initially thermally demagnetized by heating to 388 K above the Curie temperature ($T_C \approx 383$ K). The SAD were taken in the initial, demagnetized state and after step-like increase of the axial polarizing field H up to 16.5 kA/m. Two SADs were registered for each value of the applied field. After reaching the maximum H value, the polarized field was step-like reduced in the reverse sequence. As for increasing field, two consecutive measurements of the SAD were performed for each value of decreasing field. Figure 9(a) depicts the entire set of the SADs registered for increasing H. The data in Figure 9(a) correspond to the first (initial) measurement after raising the polarizing field. The behaviour of the SADs in Figure 9(a) is typical for a combination of the three components of the magnetomechanical damping, see e.g. [7,9,10,11]:

- the demagnetized state corresponds to the maximum value of the microeddy current and hysteretic non-linear damping δ_μ and δ_h, respectively. The macroeddy current damping δ_M is absent in the demagnetized state; therefore, the curve taken at 0 kA/m is characterized by relatively low low-amplitude background and the strongest non-linearity of the SAD, Figure 9(a);
- magnetization of the sample by applied field suppresses δ_μ and δ_h and promotes δ_M until the macroeddy current damping passes over the maximum at around relative net magnetization (0.6-0.7) of the saturating value; thus, the increase of the low-amplitude background in Figure 9(a) is due to the increase of the macroeddy damping component (predominant over the suppression of the microeddy term). This gradual rise of the background is combined with the suppression of the non-linearity of the SADs.

- the maximum of the low amplitude background is reached at H=15 kA/m, Figure 9(a); the non-linearity is fully suppressed by this field, as well as the microeddy current term. The disappearance of the latter cannot be directly observed in the experimental data due to the overwhelming macroeddy contribution, in contrast to the non-linear damping;
- the low-amplitude background is dominated by macroeddy contribution which is suppressed with further increase of the field; eventually, the macroeddy damping is also fully suppressed at saturation.

Now we analyze for the first time the behaviour of the decrement during increasing (direct run) and decreasing strain amplitudes (reverse run) in each SAD. The difference of damping between the direct and reverse runs is referred to as strain amplitude hysteresis [26]. The data in Figure 9(a) indicate the existence of the strain amplitude hysteresis between approximately 1.5 and 9.0 kA/m. The damping is higher for decreasing strain amplitudes than for increasing. We call this effect "positive strain amplitude hysteresis". This difference appears as soon as the strain amplitude starts to decrease in the SAD and persists down to the lowest strain amplitudes in the linear damping range. Thus, the strain amplitude hysteresis is detected either in micro- or in microeddy current damping terms. Figure 9(b) shows details of the SADs over the range of the existence of strain amplitude hysteresis (0-7.5 kA/m) on an expanded scale. In addition, the results of the second SAD scans are shown for the SADs at 3.0, 4.5 and 6.0 kA/m. Obviously, the amplitude hysteresis cannot be detected in the second run. The SAD in the second run is fully reversible and perfectly coincides with the reverse runs of the first SAD measurements. Thus, the positive strain amplitude hysteresis is a one-time effect observed only after the polarizing field increase. The hysteresis is detected only over the range of moderate polarizing fields, below the macroeddy current damping maximum.

Figure 10 shows the results of similar SAD measurements during decreasing polarizing field H. Figure 10(a) depicts the overall SAD trends for the H values between 16.5 and 0 kA/m, Figure 10(b) – details of the SAD features for moderate applied fields between 7.5 and 1.5 kA/m. The overall behaviour of the SAD is similar for increasing (Figure 9(a)) and decreasing (Figure 10(a)) field. Several important differences are:

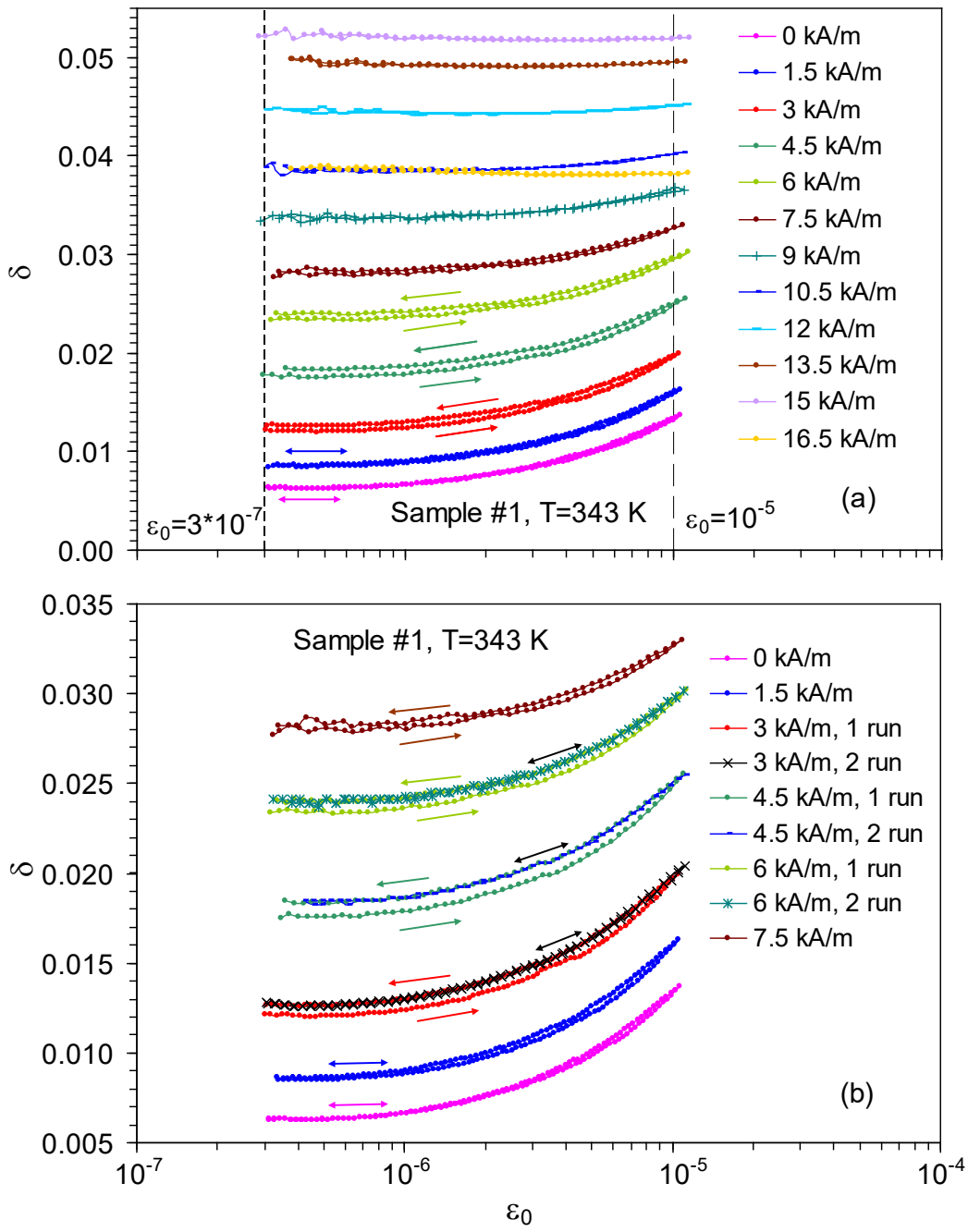

Figure 10. Strain amplitude dependence of the logarithmic decrement δ for the initially demagnetized Ni_2MnGa sample #1 at 343 K under different values of increasing polarizing magnetic field. The first measurement is shown for each value of applied field, arrows indicate the direction of the strain amplitude variation;

a) the results for the entire range of applied field from the demagnetized state up to 16.5 kA/m;

b) details of the strain amplitude dependence for low values of polarizing fields up to 7.5 kA/m; data for two consecutive runs are shown for the dependences taken at 3.0, 4.5 and 6.0 kA/m.

Dotted vertical lines in (a) mark the low and high strain amplitudes $\varepsilon_0 = 3*10^{-7}$ and $\varepsilon_0 = 10^{-5}$ for which the field dependence of the linear, total and non-linear damping terms were determined.

- for decreasing field, the low amplitude background reaches minimum no at zero applied field, but at 3 kA/m and then starts to increase for further decreasing fields of 1.5 and 0 kA/m;
- strain amplitude hysteresis is also observed during the first SAD measurement under moderate values of field, but it demonstrates a more complicated pattern. Details of the amplitude hysteresis can be appreciated in Figure 10(b) on an expanded scale. The amplitude hysteresis is detected for moderate applied field, as in the case of field increase. However, the amplitude hysteresis demonstrates cross-over phenomenon: the hysteresis is positive for high strain amplitudes in the non-linear range but becomes negative at low strain amplitudes.

The reproducibility of the regularities observed was checked for Ni_2MnGa sample #2. For this sample, the range of strain amplitudes studied was somewhat expanded both to the lower and higher values. Figure 11 depicts the results of experiments similar to the ones performed for the sample #1 (data in Figures 9 and 10). The main regularities related with the field effect on the SAD and observed for the sample #1 are fully reproduced for the sample #2. The most important feature is the inversion of the low amplitude hysteresis from positive for increasing H to negative for decreasing field, which persists in both samples.

For the sample #2 the applied field was lowered from the maximum value to 0 kA/m (which is not the demagnetized state, however) and then increased again in the opposite direction. The results of this additional test in Figure 12 confirm the re-appearance of the one-time positive strain amplitude hysteresis for increasing field of the opposite sign. Therefore, the demagnetized initial state is not a necessary condition for observation of the one-time strain amplitude hysteresis switching the sign for increasing/decreasing polarized field.

3.2. Field dependence of the linear and non-linear ultrasonic absorption

Figure 13 presents the linear and non-linear components of damping versus H derived from the data of Figure 9(a) and Figure 11(a) for the samples #1 and #2, respectively. The value of the total decrement δ is a sum of linear δ_i and non-linear δ_h terms [9]:

$$\delta(\varepsilon_0, H) = \delta_i(H) + \delta_h(\varepsilon_0, H)\,. \qquad (7)$$

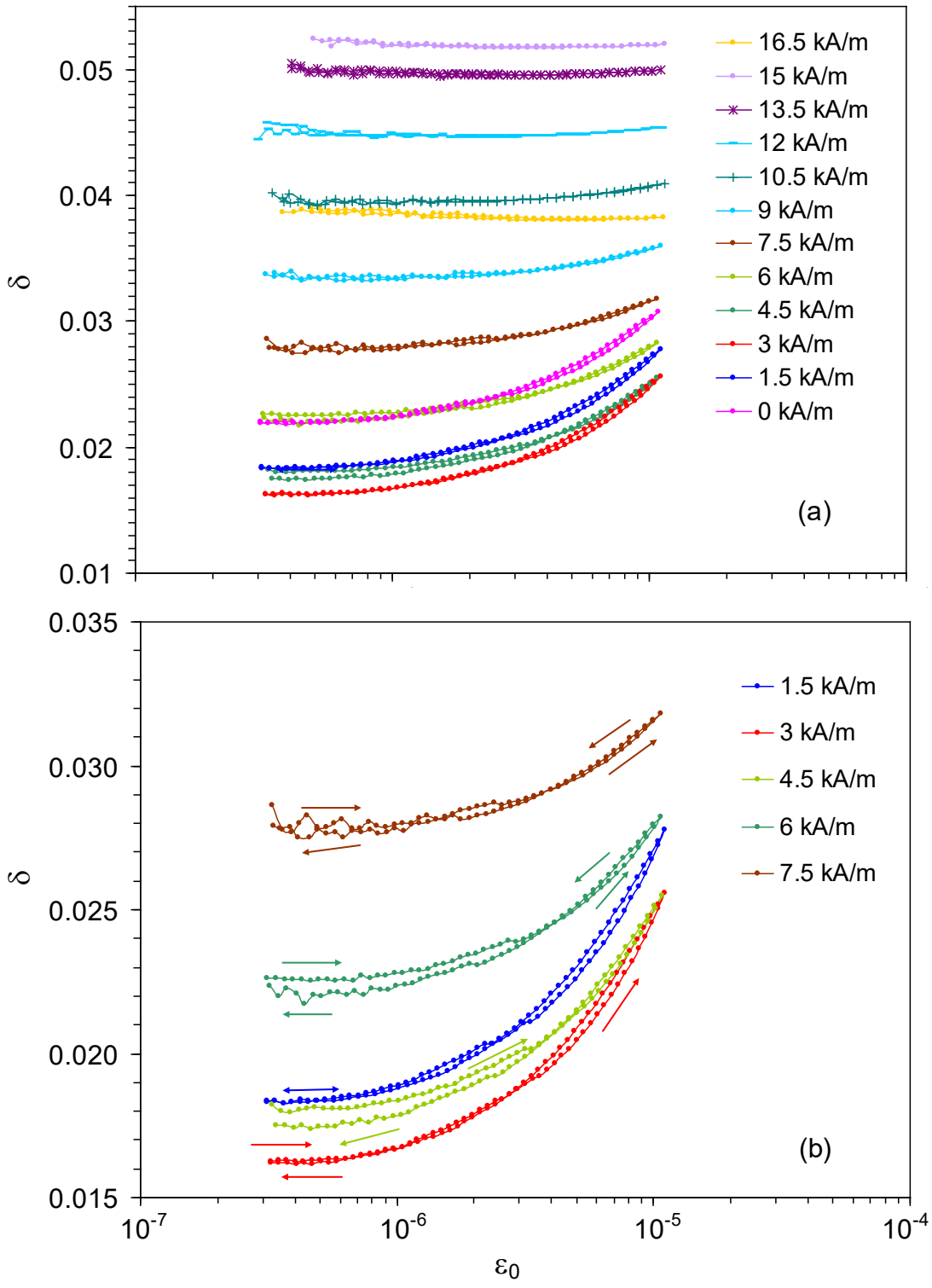

Figure 10. Strain amplitude dependence of the logarithmic decrement δ at 343 K for Ni_2MnGa sample #1 under different values of decreasing polarizing magnetic field. The first measurement is shown for each value of applied field, arrows indicate the direction of the strain amplitude variation;
a) the results for the entire range of applied field from 16.5 to 0 kA/m;
b) details of the strain amplitude dependence for low values of polarizing fields below 7.5 kA/m.

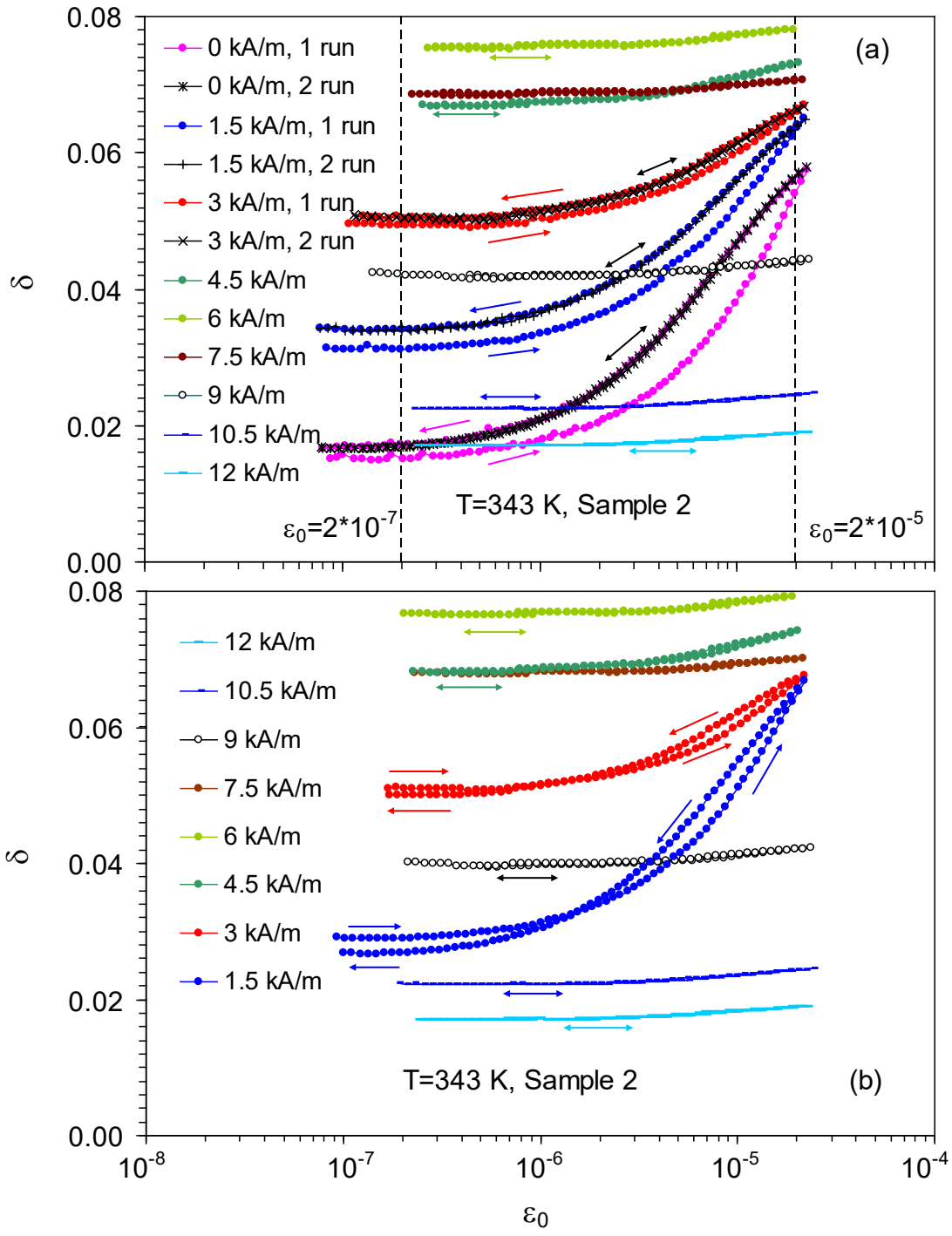

Figure 11. Strain amplitude dependence of the logarithmic decrement δ at 343 K for Ni_2MnGa sample #2 under different values of increasing (a) and decreasing (b) polarizing magnetic field. The first measurement is shown for each value of applied field, except for the field of 0, 1.5, 3.0 kA/m for increasing field (panel (a)), where the data for two consecutive runs are shown. The arrows indicate the direction of the strain amplitude variation. Dotted vertical lines in (a) mark the low and high strain amplitudes $\varepsilon_0 = 2*10^{-7}$ and $\varepsilon_0 = 2*10^{-5}$ for which the field dependence of the linear, total and non-linear damping terms were determined.

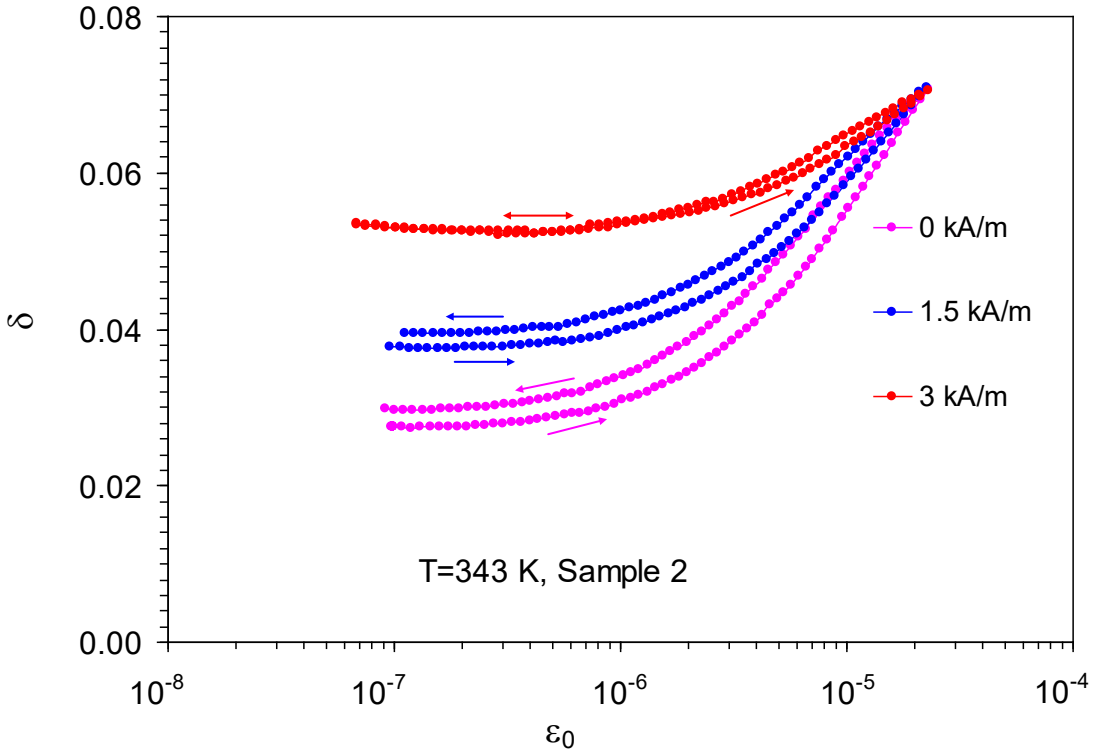

Figure 12. Strain amplitude dependence of the logarithmic decrement δ at 343 K for Ni_2MnGa sample #2 under different values of increasing polarizing magnetic field. The first measurement is shown for each value of applied field, except for the field of 0, 1.5, 3.0 kA/m for increasing field (panel (a)), where the data for two consecutive runs are shown. The arrows indicate the direction of the strain amplitude variation.

If the damping of non-magnetic origin is neglected in Ni_2MnGa [11], the linear term is, in turn, a sum of micro- and macroeddy current components, δ_μ and δ_M, respectively:

$$\delta_i(H) = \delta_\mu(H) + \delta_M(H). \tag{8}$$

The macroeddy damping vanishes in the demagnetized state and the linear damping represent the microeddy current damping:

$$\delta_i\big|_{H=0} = \delta_\mu\big|_{H=0} \tag{9}$$

The linear damping term δ_i, for each value of H, was determined directly from the experimental data for the lowest strain amplitude $\varepsilon_0 = 3*10^{-7}$ for the sample #1 and

ε_0=2*10^{-7} for the sample #2. The non-linear term was derived using Eq. 7 as a difference between experimentally determined total damping (at strain amplitude ε_0=10^{-5} for sample #1 and ε_0=2*10^{-5} for the sample #2) and linear damping δ_i:

$$\delta_h(\varepsilon_0) = \delta(\varepsilon_0) - \delta_i . \qquad (10)$$

The low and high strain amplitudes selected for the samples #1 and #2 are marked in Figures 9(a) and 11(a), respectively.

Thus determined linear and non-linear damping terms demonstrate canonical behaviour [7,11]:

- the linear term shows a maximum due to the macroeddy component;
- the non-linear damping is suppressed with field; a slight maximum is detected for the sample #2, similar to the report by Coronel and Beshers [7];
- the non-linear damping is essentially suppressed for the H value corresponding to the macroeddy current damping maximum.

Quantitative differences between sample #1 and sample #2 are as follows:

- the maximum of the linear damping and the suppression of the non-linear one occurs at ca. 2 times higher field for the sample #2 than for the sample #1;
- the non-linear damping values are notably higher for the sample #2 than for the sample #1.

The first difference points to the higher saturating H values H_{sat} for the sample #1. Two reasons of the higher H_{sat} for the sample #2 exist: (i) the sample #2 is nearly two times longer than the sample #1 (11.68 mm against 6.28 mm); therefore, the demagnetizing factor is higher for the shorter sample #1; (ii) surface damage of the sample #1, which was slightly grinded after magnetic permeability measurements, whereas the sample #2 was chemically polished. Surface defects can increase H_{sat}.

Figure 14 shows strain amplitude dependence of the non-linear part of damping δ_h at 343 K and different polarizing fields H for the sample #1 (a) and #2 (b). Each dependence for different values of H was derived using Eq. 10. The data on log-log scale show essentially a monotonous decrease with field consistent with Figure 13. A small maximum at low field for the sample #1 is not resolved. For the sample #1 the dependences are linear on log-log scale over the entire range of strain amplitudes scans

with the slope close to 1. Thus, the SAD is a power law $\delta_h(\varepsilon_0) \propto \varepsilon_0^n$ with the exponent $n \cong 1$, characteristic of the Rayleigh law in ferromagnetics [10,7]. The sample #2 shows

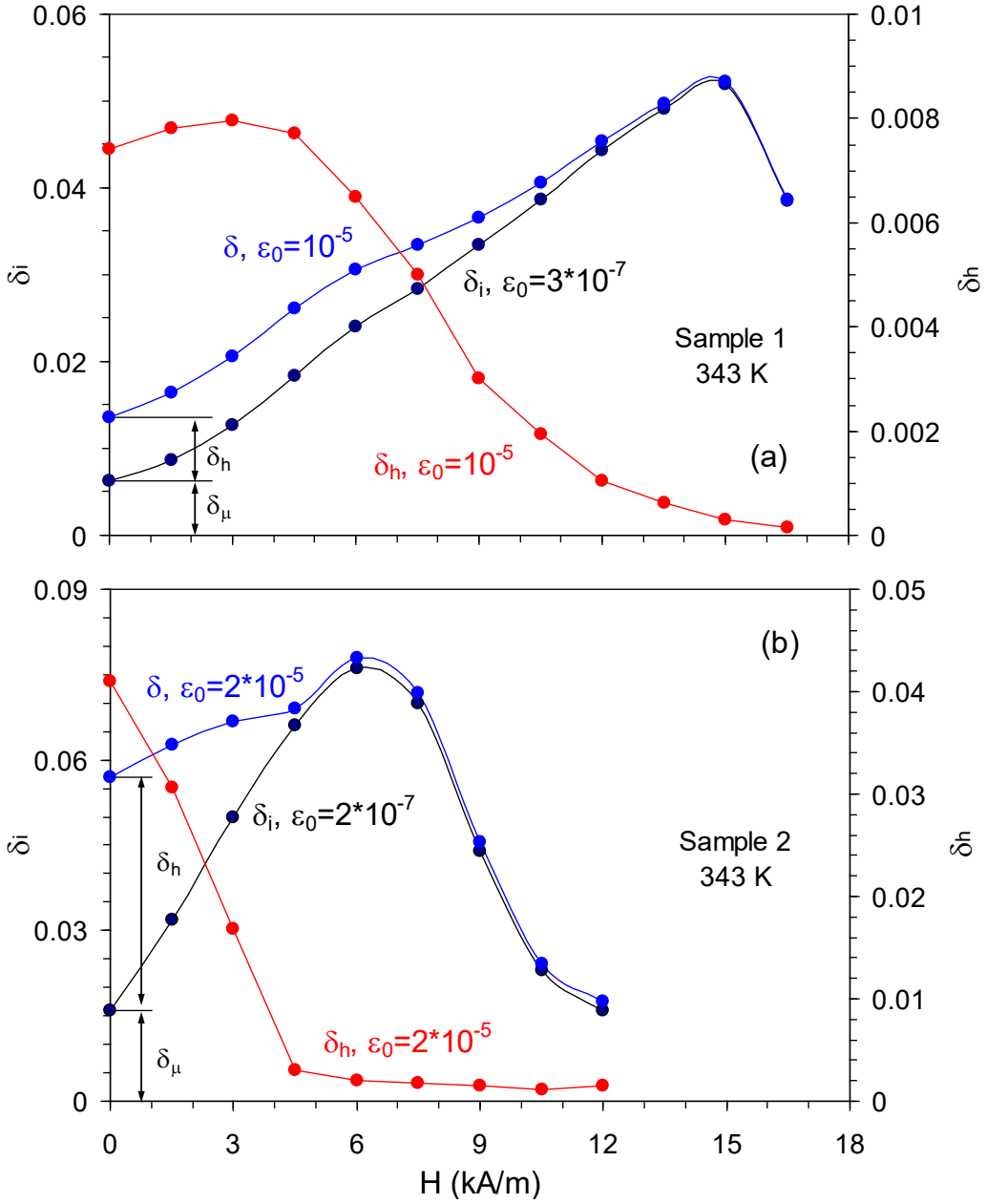

Figure 13. The total δ and linear δ_i damping at high and low strain amplitudes and their difference, the non-linear component δ_h of the total damping, versus polarizing field H for temperature T=343 K. Linear damping is determined for the low strain amplitude ε_0=3*10^{-7}, the total and non-linear damping for the high strain amplitude ε_0=10^{-5} for the sample #1 (a), the low and high strain amplitudes were ε_0=2*10^{-7} and ε_0=2*10^{-5}, respectively, for the sample #2 (b). The decomposition of the total damping for the demagnetized state at H=0 into the linear microeddy current δ_i and non-linear hysteretic damping δ_h is shown.

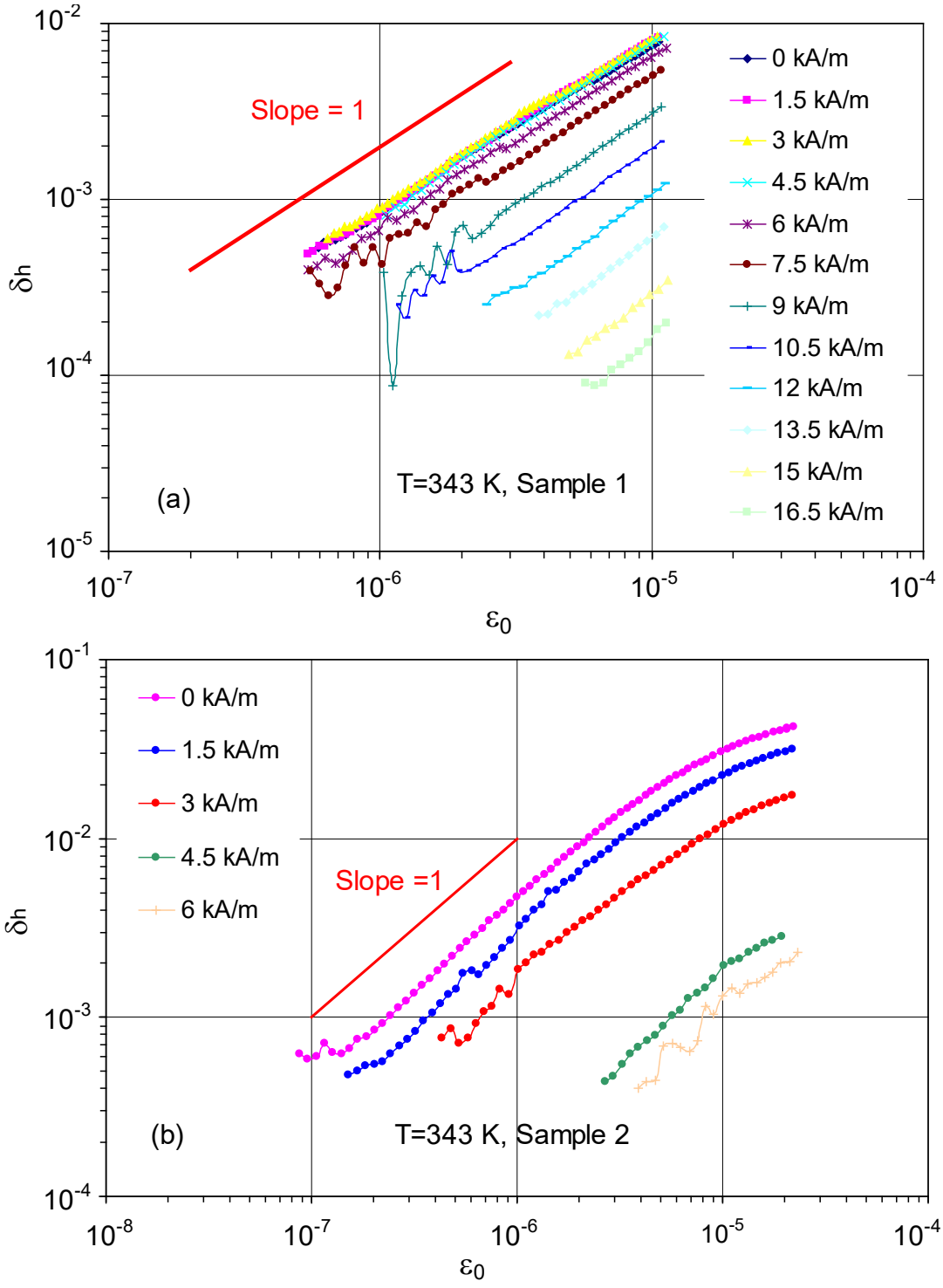

Figure 14. Strain amplitude dependent part of the logarithmic decrement δ_h at 343 K for Ni_2MnGa samples #1 (a) and sample #2 (b) versus strain amplitude ε_0 under different values of increasing polarizing magnetic field. The data are shown for increasing strain amplitudes during the first run for each value of applied field.

the saturation of δ_h at highest strain amplitudes in the so-called super Rayleigh region [7]. The saturation represents an onset of the expected δ_h maximum versus ε_0 [10].

Summary and discussion of Sections 3.1. and 3.2.

Single crystalline samples of stoichiometric Ni_2MnGa demonstrate canonical behaviour in terms of the effects of applied field and strain amplitude on the three components of magnetomechanical damping: (i) the monotonous decrease of microeddy current and hysteretic damping with field and the maximum of macroeddy current damping; (ii) power law SAD of the hysteretic term with a slope n=1. Our main interest will be focussed on the mechanisms of the new phenomenon uncovered: one-time strain amplitude hysteresis of damping in the low-amplitude range of linear damping. The data analyzed point to the superposition of two components of the strain amplitude hysteresis: (i) the positive one both for increasing and decreasing field over the range of non-linear damping and (ii) the hysteresis in the linear range of damping, which is positive for increasing field and negative for the decreasing one. Positive strain amplitude hysteresis in the non-linear range of magnetomechanical damping was observed by Beshers [7], without elaborated interpretation. One-time low amplitude hysteresis provoked by variations of field has not been reported as far as we are aware. To begin with, we mention that the uncovered hysteresis is the one-time effect and is not associated with any time dependence of the damping contrary to the classical observations initiated by Chambers and Smoluchowski [26]. Therefore, the hysteresis is not related with any diffusion-controlled redistribution of obstacles by oscillating DWs and needs a new interpretation. Since the total damping in the cubic phase of Ni_2MnGa is predominantly of magnetomechanical origin [11], the origin of this hysteresis is in the variation of either microeddy or macroeddy current damping terms, provoked by a combined action of applied field and ultrasonic oscillations in the non-linear range. The first important point is that non-linear ultrasonic oscillations are related with the relatively large-scale motion of non-180 degrees magnetic domain walls. At the same time, the magnetization-field M(H) trajectory of a ferromagnet for increasing and decreasing field is the magnetic hysteresis [8]. The hysteresis, in its turn, reflects the sequence of non-equilibrium states of magnetic domain walls [8]. Therefore, it can be assumed, as a working hypothesis, that the oscillatory motion of the domain walls in the range on non-linear anelasticity provokes their relaxation into the deeper energy minima closer to the equilibrium state. The key issue here is the change of the type of the hysteresis for increasing and decreasing field. It is suggested that after increasing/decreasing the field the domain walls are trapped by the obstacles in

configurations that impede their motion and do not allow them to arrive at the equilibrium magnetization value under the action of static local field. Obviously, this equilibrium value is higher than reached for increasing field and lower than reached for the decreasing field. Then, the combined action of the static local field and non-linear ultrasonic oscillations trigger the motion of the domain walls towards their new positions, closer to the equilibrium configuration. The "activation" of the domain wall irreversible motion thus provokes the increase of the net magnetization of the sample for the series of increasing H steps and the decrease of the net magnetization for the series of decreasing H steps. The change of the net magnetization (for low and moderate fields) provokes the change of the macroeddy current damping term. This is the reason of one-time increase of δ_i for increasing H steps and of the one-time decrease of δ_i for decreasing H-steps. The relation between the magnetization and macroeddy current damping controlled δ_i exemplified by the data in Figure 13, accounts for the change of the sign of the hysteresis under increasing and decreasing H steps. The second and the following measurements of the SAD do not produce an additional magnetization change, explaining the one-time property of the hysteresis.

Another strong argument supporting suggested interpretation is the observation of strain amplitude hysteresis only at moderate values of decreasing and increasing polarizing field. Studies of the Barkhausen noise intensity, see e.g. Fig. 9.10 of Reference 8, indicate that this range corresponds to the most intense rearrangement of DW structure. Strain amplitude hysteresis vanishes with increasing field in parallel with the suppression of the non-linear hysteretic damping when the DW density diminishes. The strain amplitude hysteresis disappears at high fields close to saturation, when disappears the hysteresis in M(H) curve.

The suggested interpretation of the low-amplitude hysteresis implies additional activation of the domain wall mobility by the ultrasonic oscillations in the non-linear range. Therefore, one should expect narrower magnetic hysteresis if non-linear oscillations of domain walls are excited in the sample as compared to the sample without oscillations. To check this prediction we will use the mechanomagnetic spectroscopy method applied to the same samples #1 and #2. This method does not allow one to obtain M(H) hysteresis, but yields the hysteresis of reversible inverse magnetostriction (reversible Villari effect, RVE) versus H. Since the zero RVE points correspond to zero net magnetization of the sample [27,28] the width of the RVE

hysteresis yields the coercive force H_c as a distance between the H values wherein the net magnetization of the sample vanishes. Thus, to verify our working hypothesis, one has to register RVE versus H hysteresis and compare the width of the loops with and without non-linear oscillations. This is the subject of the next two Sections.

3.3. Temperature dependence of the reversible inverse magnetostriction

In the following two sections we will check whether the mechanical oscillations in the range of non-linear motion of magnetic domain walls reduce the coercive field. We will study hysteresis of the reversible inverse magnetostriction or reversible Villari effect by means of the mechanomagnetic spectroscopy, introduced in Section 2.2.

To begin with, one has to prove that the reversible inverse magnetostriction signal does not contain any substantial leakage or parasitic signal induced by rather high excitation voltage of the transducer. To confirm the magnetic origin of the RVE signal we perform the temperature scans with the highest temperature above the Curie temperature T_C of the material. If the signal has the magnetic origin (as expected) it should disappear in the paramagnetic state of the material.

Figure 15 shows the temperature spectra of the amplitude of the first harmonic of the RVE signal B_m for the two samples, #1 and # 2. The oscillatory strain amplitude was maintained at $2*10^{-7}$ and external magnetic field was not applied, H=0. The samples were initially in the magnetized state at room temperature. Data in Figure 15 point to an abrupt drop of the RVE on heating at around 383 K, the Curie temperature of the material. The RVE signal becomes negligible above T_C. Upon cooling, the RVE signal rises at T_C, although the polarizing field was not applied and RVE should vanish for zero net magnetization. The RVE signal on cooling under H=0 is much lower than during heating of the sample in the remanent state. This weak RVE signal should be attributed to the weak uncompensated magnetic field that exists in the laboratory and magnetic field of the Earth.

This conclusion is confirmed comparing the data on heating for the demagnetized state of the sample and RVE during field cooling under H=3.0 kA/m, presented in Figure H. RVE during zero field cooling, Figure 15, is on the order of 10 nT for T=(300-370) K. According to Figure 16, the RVE under H=3.0 kA/m is ca. 1000 nT. Assuming, as a first approximation, that for low field values $B_m \propto H$ (the validity

of this assumption will be confirmed later on), the value of the background field (under H=0) is ca. 30 A/m. This is precisely the value of the Earth magnetic field [29] ranging from 0.25 to 0.65 G (20 to 50 A/m).

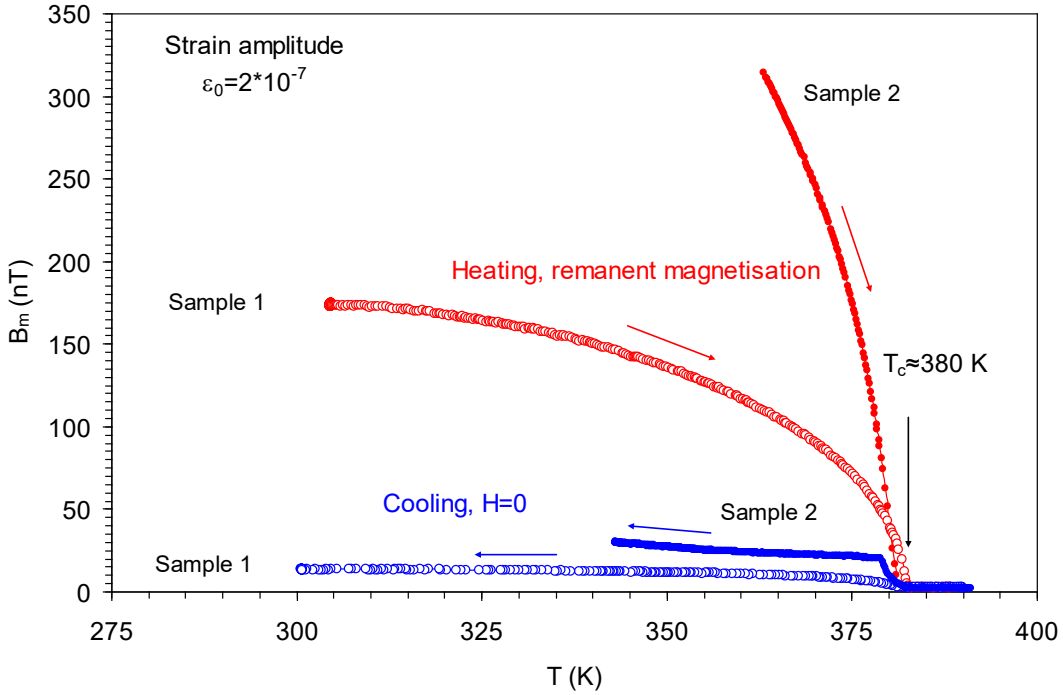

Figure 15. Temperature spectra, close to the Curie temperature $T_c \approx 383$ K, of the amplitude of the reversible inverse magnetostriction (reversible Villari effect) B_m for the Ni_2MnGa samples # 1 and # 2 on heating in the remanent state and on cooling from above the T_C under zero applied field. Oscillatory strain amplitude $\varepsilon_0=2*10^{-7}$.

The data in Figure 16(a) deserve further comment. First, upon cooling from the paramagnetic state, RVE shows a sharp peak, levels off at ca. 360 K and remains essentially constant down to the temperature of premartensitic transformation at ca. T_{pm}=260 K. The peak just below T_C is associated with the increase of the saturating field upon cooling the ferromagnet below T_C as will be explained later. Second, the peak of magnetostriction at T_{pm} is responsible for the internal friction peak. A combination of the magnetostriction peak and sharp decline of the permeability at T_{pm} yields splitting of the damping peak at T_{pm} [16]. Third, the ferromagnetic ordering at T_C is the second order transition and does not show temperature hysteresis. The premartensitic transition is weakly first order and is characterized by a clearly detectable temperature hysteresis of ca. 1 K. Fourth, Figure 16(b) shows details of the RVE upon zero field heating and field cooling. The RVE shows a discontinuity of the first derivative during zero field cooling, which yields the correct T_C value. Application

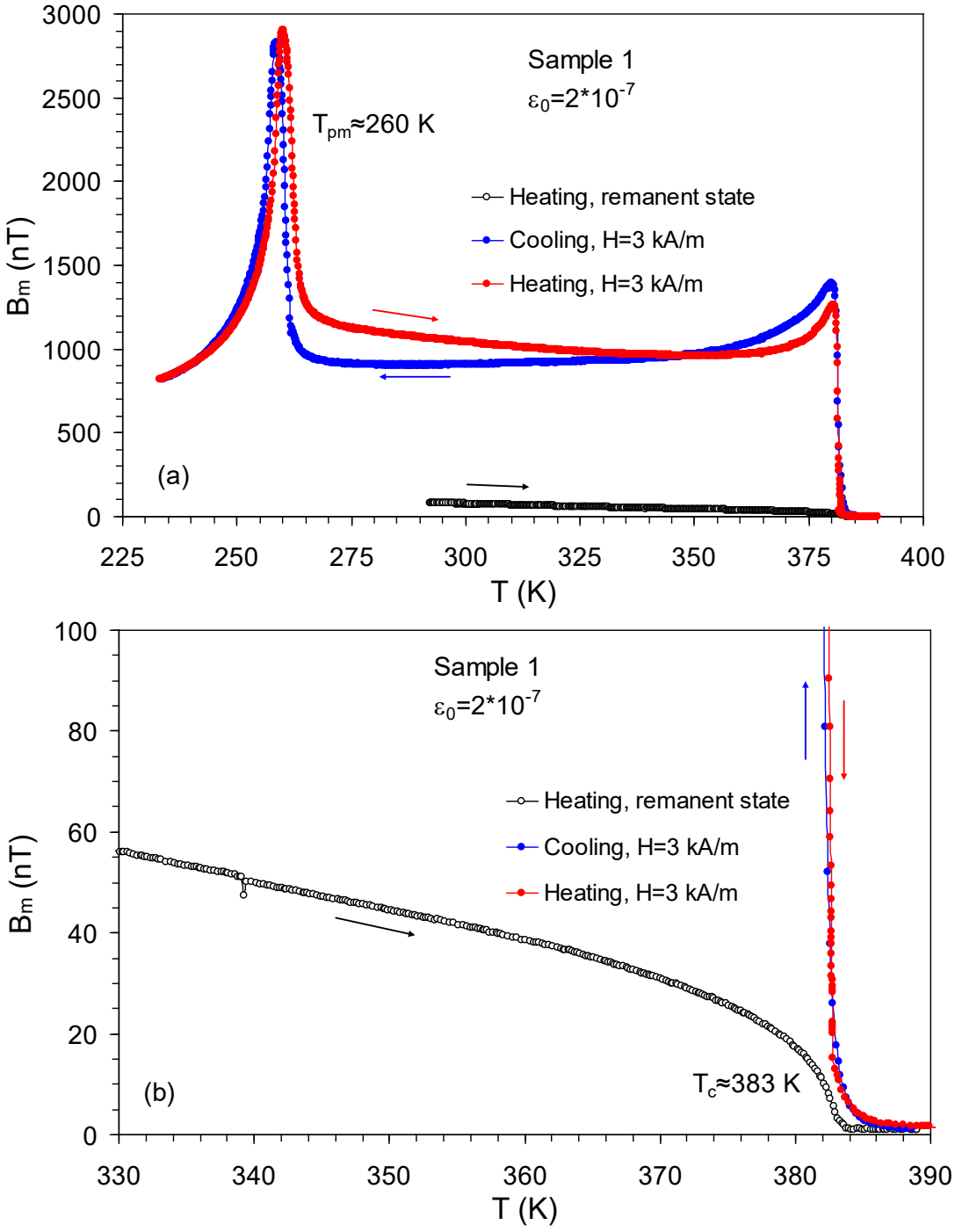

Figure 16. Temperature spectra of the amplitude of the reversible inverse magnetostriction (reversible Villari effect) B_m for the Ni_2MnGa sample # 1 on first heating in the remanent state (black symbols) and on consecutive cooling-heating cycle between 390 K (above the Curie temperature T_C) and 230 K (below the premartensitic transition temperature T_{PM}) under applied field of 3.0 kA/m. Strain amplitude ε_0=2*10^{-7}.
a) Overall temperature spectra between 230 and 390 K;
b) details of the spectra close to the Curie temperature on an expanded scale.

of the field during cooling removes the discontinuity and shifts the RVE spectrum to higher temperature. As is well known, that is the reason why temperature spectrum of magnetization under applied field does not yield directly the T_C value and require construction of so-called Arrot plots [5].

Thus, RVE data should yield reliable data for determining the coercive field from the magnetic field hysteresis of the reversible inverse magnetostriction.

3.4. Effect of ultrasonic oscillations on magnetoelastic hysteresis

Figure 17 shows the hysteresic loops of real part of the first harmonic of RVE, B_0, versus H registered at 343 K for the sample #1. Two hysteretic loops were registered for the low oscillatory strain amplitudes belonging to the range of small domain wall displacements in the linear mode, $\varepsilon_0 = 2*10^{-7}$, and for high strain amplitude, $\varepsilon_0 = 10^{-5}$, well in the range of non-linear domain wall dynamics. Each hysteresis loop (HL) consists of 100 experimental points. Several points deserve mentioning as far as the general HL configuration is concerned, Figure 17(a). First, each HL shows two sections, at low and high values of the field. The low-field section extends up to approximately 5 kA/m. It is characterized by smooth shape and counter clockwise rotation. The shape of the two high-amplitude parts of the HLs is less regular (jerky) and shows clockwise rotation. The unusual direction of rotation is allowed in mixed variables, since the area of the loop does not represent the energy dissipated. The variation of the rotation is reported for Ni-Fe-Ga ferromagnetic shape memory alloy [30] and various ferroelectrics [31]. In addition, the slopes of the loops change in the crossover points, wherein the directions of the HL rotation change. The data available are not sufficient to interpret these intriguing features of the HLs and our goal is merely to compare the width of the HLs with and without high-amplitude ultrasonic excitation. Figure 17(b) shows the central parts of the two HLs on an expanded scale. Although the width of the loops is rather small, Figure 17(b) indicates that the HL registered with high-amplitude excitation is inside the HL under low-amplitude excitation. We mention also that the RVE scales very well with the strain amplitude ε_0: the difference between low and high strain amplitudes is 50 times which is the same as the scaling factor in Figure 17. Thus, the experiment at 343 K for the sample #1 confirms our prediction of

the more equilibrium state of domain walls subjected to the high amplitude ultrasonic oscillations.

Similar experiments with the sample #1 were performed at two additional temperatures: 303 K, in the cubic phase and at 250 K, in the premartensitic one. The corresponding results are shown in Figures 18 and 19, respectively. The data for 303 and 250 K are qualitatively similar to the results obtained at 343 K. Minor differences are related with the decrease of temperature: (i) higher maximum B_0 values (note different ordinate scales in Figures 17, 18, 19); (ii) decreasing the change of the slope of the HL in the cross-over points, which disappears at 250 K; (iii) decrease of the cross-over field and coercive field at 250 K. The interpretation of all these minor details is beyond the scope of the present work. Despite these minor differences, the crucial observation that the width of the hysteresis diminishes when the field variation is combined with ultrasonic oscillations in the non-linear range is preserved. The existence of the same regularity was checked for the sample #2. Similar HLs registered for the sample #2 at 343 K are shown in Figure 20. In contrast to sample #1, the RVE for sample #2 shows a maximum at ca. 5 kA/m and declines at higher applied fields, Figure 20(a). The decrease of the RVE towards zero values is a typical at saturation [30]. This difference between the RVE for samples #1 and #2 agrees with the lower applied saturating fields for the sample #2, exemplified by the data in Figure 13. It is quite remarkable that the HLs are jerky over the intermediate range of applied field and become smooth at low applied field and close to saturation. Another feature is the emergence of a new cross-over point at a value of applied field ca. 6.5 kA/m, separating opposite directions of the circulation along the HLs. Thus, each branch of the HLs has two cross-over points at 1 and 6.5 kA/m. Thus, the direction of the circulation along the loop changes twice up to the saturating field. Figure 20(b) shows the results of the experiments for which the maximum applied field was limited to 4.5 kA/m. This experiment permitted determining details of the RVE behaviour at relatively low fields The data in Figure 20(b) confirms the existence of the cross-over point at ca. 1 kA/m and the expansion of the central part of the HLs (Figure 20(c)) clearly indicates that the high-amplitude HL falls within the low-amplitude HL. Thus, the reduction of the magnetic hysteresis by ultrasonic oscillations is confirmed for the sample #2.

Summary and discussion of Sections 3.3. and 3.4. General comments.

Studying of the RVE hysteresis confirms the hypothesis that ultrasonic oscillations in the range of non-linear domain wall dynamics relaxes the domain walls into a configuration closer to the equilibrium.

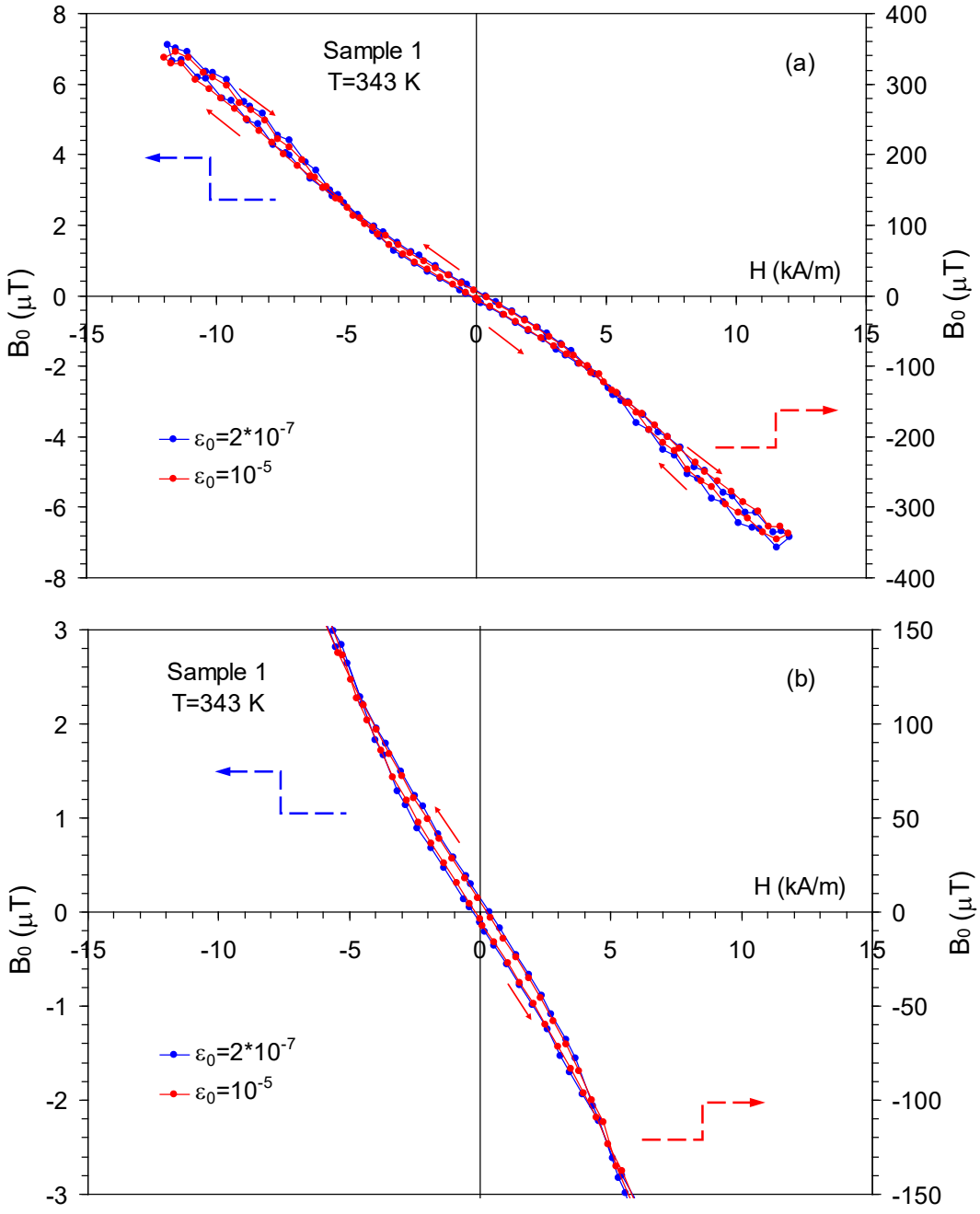

Figure 17. Real part of the first harmonic of reversible inverse magnetostriction B_0 (reversible Villari effect) versus cyclic polarizing field (frequency of the cycle 0.001 Hz) for the Ni_2MnGa sample # 1. Measurement at 343 K at two different strain amplitudes $\varepsilon_0=2*10^{-7}$ and $\varepsilon_0=10^{-5}$:
a) entire hysteresis loops for the field H between -12 and 12 kA/m;
b) central parts of the loops on an expanded scale.

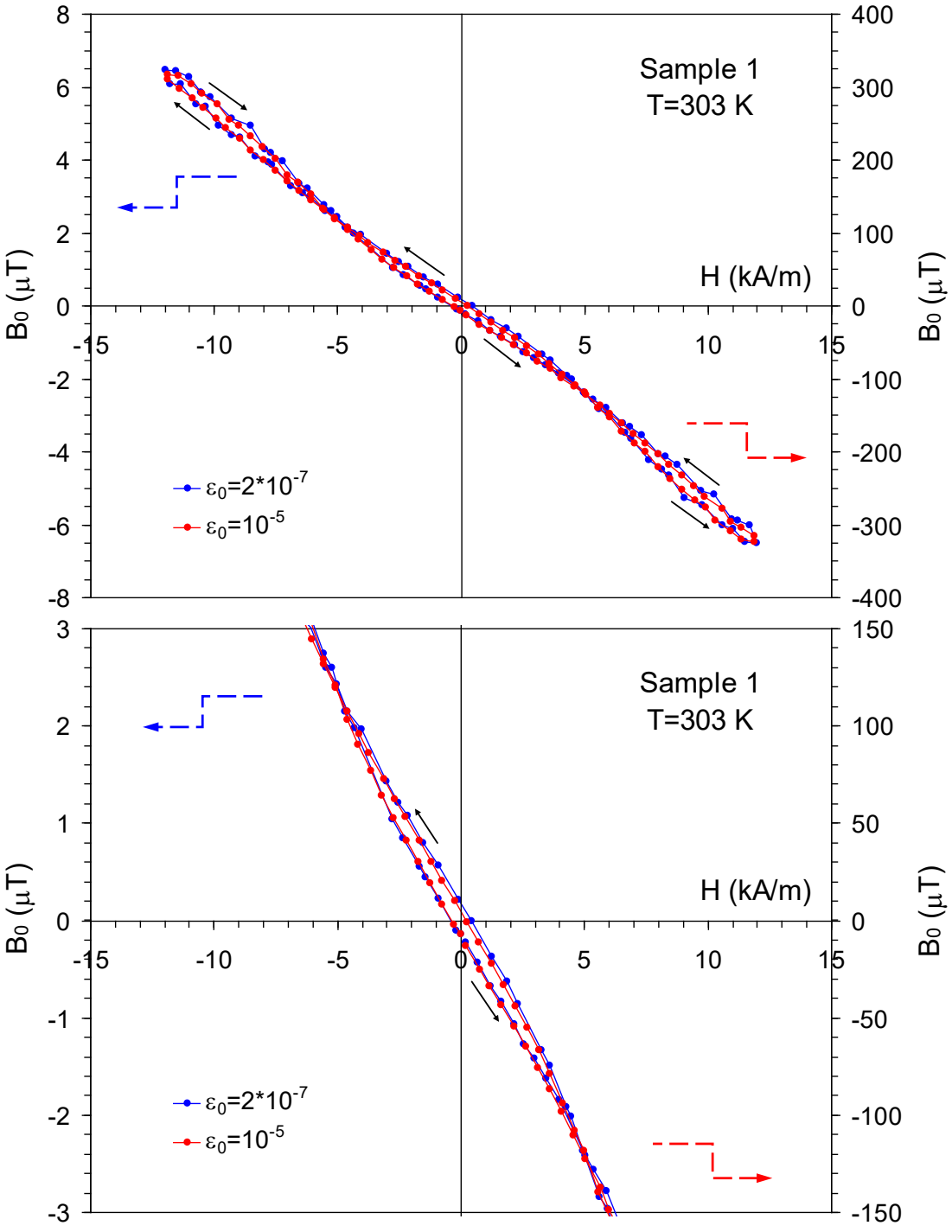

Figure 18. Real part of the first harmonic of reversible inverse magnetostriction B_0 (reversible Villari effect) versus cyclic polarizing field (frequency of the cycle 0.001 Hz) for the Ni_2MnGa sample # 1. Measurement at 303 K at two different strain amplitudes $\varepsilon_0=2*10^{-7}$ and $\varepsilon_0=10^{-5}$:
a) entire hysteresis loops for the field H between -12 and 12 kA/m;
b) central parts of the loops on an expanded scale.

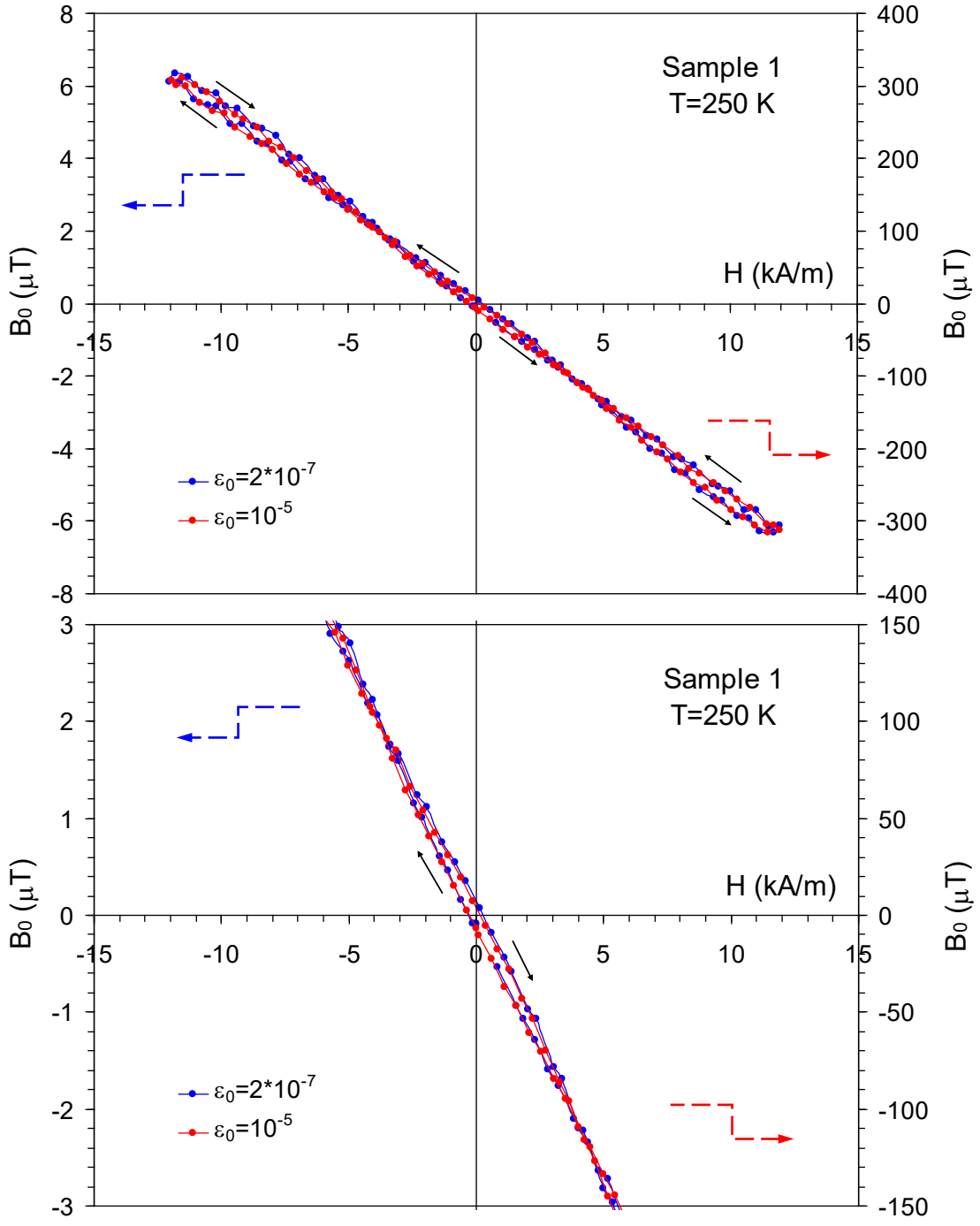

Figure 19. Real part of the first harmonic of reversible inverse magnetostriction B_0 (reversible Villari effect) versus cyclic polarizing field (frequency of the cycle 0.001 Hz) for the Ni_2MnGa sample # 1. Measurement at 250 K at two different strain amplitudes $\varepsilon_0=2*10^{-7}$ and $\varepsilon_0=10^{-5}$:
a) entire hysteresis loops for the field H between -12 and 12 kA/m;
b) central parts of the loops on an expanded scale.

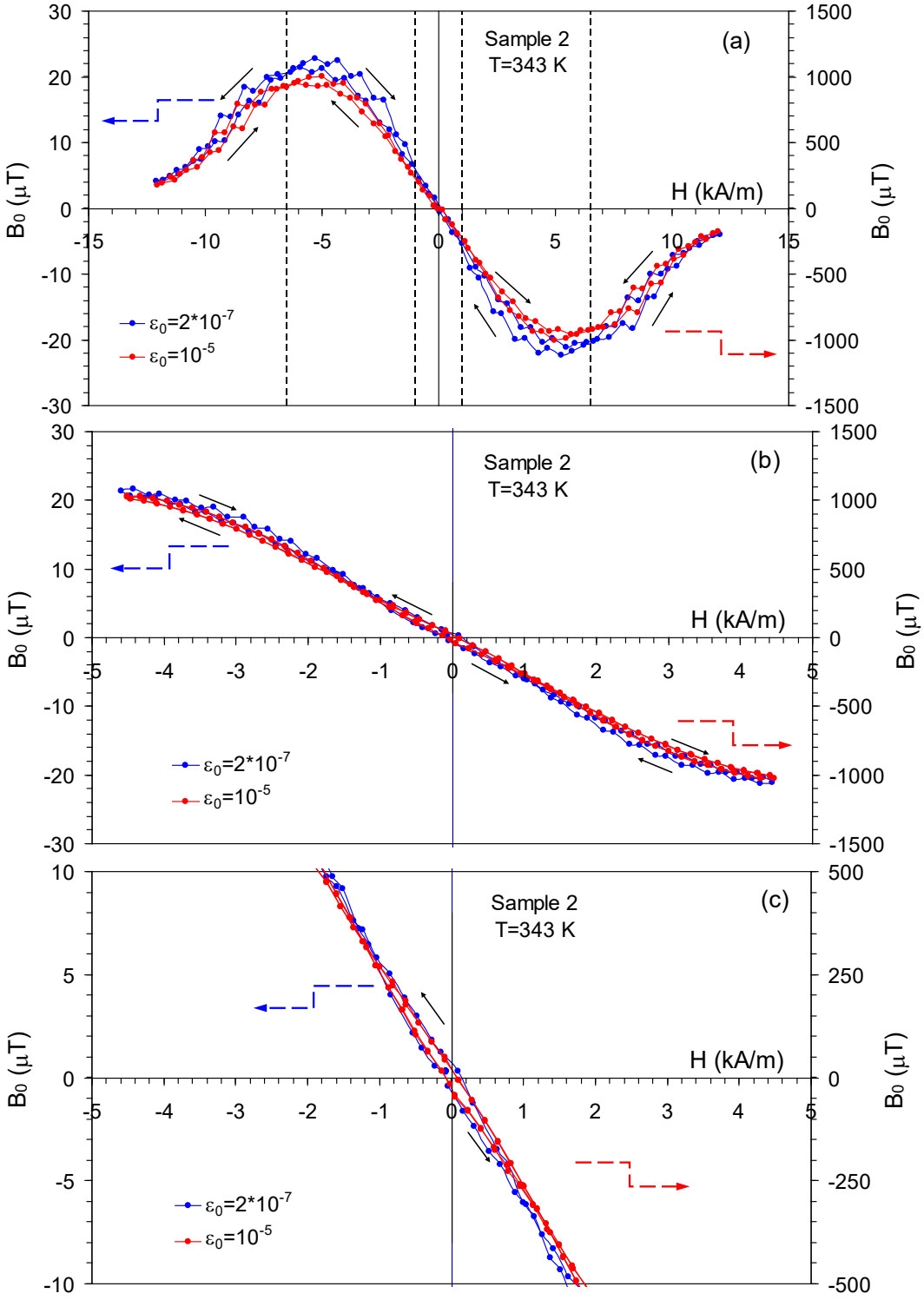

Figure 20. Real part of the first harmonic of reversible inverse magnetostriction B_0 (reversible Villari effect) versus cyclic polarizing field (frequency of the cycle 0.001 Hz) for the Ni_2MnGa sample # 2. Measurement at 343 K at two different strain amplitudes $\varepsilon_0=2*10^{-7}$ and $\varepsilon_0=10^{-5}$:
a) hysteresis loops for the field H between -12 and 12 kA/m; thin dotted lines mark the cross-over points wherein the direction of the circulation along the loop changes.
b) hysteresis loops for the field H variation between -4.5 and 4.5 kA/m;
c) central parts of the loops from (b) on an expanded scale.

This relaxation is a one-time effect when the domain walls are trapped in local energy minima after a step-like increase of the polarizing field and is a continuous phenomenon when a continuous magnetic field ramp is applied to a sample. The phenomenon of the relaxation of domain wall configuration can be reformulated in terms of the net magnetization of the sample: the superposition of ultrasonic oscillations additionally increase the net magnetization under raising field and decrease it when the applied field diminishes. The effect of superposition of the ultrasonic oscillations is known for mechanical deformation of crystals. Conventional dislocation plasticity is promoted by oscillations in a Blaha-Langeneker effect [32,33], referred to also as acoustoplastic effect. Superposition of the ultrasonic oscillations on quasistatic stress reduces the yield and flow stresses due to the extra plastic strain induced by such superposition. Ultrasonic oscillations promote also pseudoelastic strain during direct and reverse martensitic transformation [34] (acoustopseudoelastic effect). The last effect results in a reduction of the stress-pseudoelastic strain hysteresis in Cu-Al-Ni single crystals [34]. Both previous phenomena involve the additional strain under superposition of oscillatory and static stress. In the present work we report fundamentally similar effect, but observed for mixed variables: superposition of mechanical oscillations and static magnetic field affect the magnetization of the sample. In a way analogous to acoustoplastic and acoustopseudoelastic effects, the phenomenon uncovered in the present work can be coined “acoustomagnetic effect”.

Mixed variables involved in acoustomagnetic effect can be reduced to conjugate ones using basics of the magnetoelastic coupling phenomenon. In fact, magnetomechanical damping is a manifestation of such coupling related to the stress-induced motion of magnetic domain walls and, hence, dissipation of energy. The equivalence between the applied stress and magnetic field is expressed using so-called stress anisotropy field. For an isotropic ferromagnet with saturation magnetization M_s and magnetostriction λ_s, the applied stress s creates stress anisotropy field H_σ [5]:

$$H_\sigma \cong \frac{3}{2}\frac{\sigma\lambda_s}{\mu_0 M_s}. \qquad (11)$$

The stress anisotropy field thus creates the magnetization change ΔM :

$$\Delta M = \Delta M(H_\sigma). \qquad (12)$$

Equations (11) and (12) yield the phenomenological interpretation of the acoustomagnetic effect. An important issue raised in the microscopic interpretation of the acoustoplastic and acoustopseudoelastic effects is related to the possibility to apply the superposition principle to the ultrasonic and quasistatic stresses [33,34]. Experimental data point to the existence of the critical stresses in acoustoplastic and acoustopseudoelastic effects that might prove that the superposition principle is not applicable at low oscillatory stress amplitudes. The reason of the failure of superposition is ascribed to the necessity for the ultrasonic oscillations to be intense enough (in other words, to have sufficient amplitude) to provoke depinning of dislocations (conventional plasticity) or twin boundaries (superelastic strain in transformation plasticity) in order to contribute to the additional macroscopic strain. Therefore, the occurrence of the acoustoplastic and acoustopseudelastic effects was exclusively restricted to the range of strain amplitudes wherein anelasticity is strongly non-linear.

The present results are not sufficient to contribute to the similar analysis of the acoustomagnetic effect. Nevertheless, it is instructive to estimate the corresponding values of the stress anisotropy field for the cubic Ni_2MnGa. We will rewrite Equation (11) for the anisotropy field amplitude H_{σ_0} using experimental values of the oscillatory strain amplitude ε_0:

$$H_{\sigma_0} \cong \frac{3}{2}\frac{\varepsilon_0 E \lambda_s}{\mu_0 M_s}, \qquad (13)$$

where E is the Young´s modulus.

We will estimate H_{σ_0} for the two values of strain amplitude, $\varepsilon_0 = 2*10^{-7}$ and $\varepsilon_0 = 10^{-5}$. If one takes $E \approx 10$ GPa [11], $\lambda_s \approx 50*10^{-6}$ [35] (we note that the magnetostriction λ_s is negative), $\mu_0 M_s \approx 0.5$ T, Figure 5 and Reference 19, a negligible value $H_{\sigma_0} \approx 0.3$ A/m is obtained for $\varepsilon_0 = 2*10^{-7}$. The strain amplitude $\varepsilon_0 = 10^{-5}$ yields $H_{\sigma_0} \approx 15$ A/m. This value is two orders of magnitude lower than the applied field

step of 1.5 kA/m for the experiments with sample #1 and sample #2, see Figures 9 and 11. Therefore, assuming the linear dependence of macroeddy (more precisely, of the sum of micro- and macroeddy) damping on applied field, Figure 13, one should expect the magnitude of the hysteresis approximately 0.01 of the damping variation induced by the field step. The data in Figures 9 and 11 indicate that the magnitude of the hysteresis is an order of magnitude higher. This analysis supports the hypothesis that the ultrasonic oscillations locally activate the motion of domain walls trapped in local energy minima. Therefore, the effect of superposition of the ultrasonic oscillations is stronger than simple superposition of static and periodic stress anisotropy field.

4. Summary and conclusions

- Systematic studies have been performed of the linear and non-linear components of the ultrasonic magnetomechanical internal friction in single crystalline samples of Ni_2MnGa ferromagnetic shape memory alloys in the cubic phase under step-like variations of polarizing magnetic field.

- A new effect of one-time hysteresis in the linear component of the magnetomechanical damping provoked by step-like variations of the polarizing field is found. It is shown that the sign of the hysteresis is different for increasing and decreasing polarizing field.

- It is suggested that the uncovered hysteresis is due to macroeddy component of magnetomechanical damping, controlled by the net magnetization of the sample. The one-time hysteresis of different signs for increasing and decreasing field is associated with additional increase/decrease of magnetization that stems from the relaxation of magnetic domain walls trapped in metastable states. The relaxation is "triggered" by ultrasonic oscillations.

- In analogy with similar phenomena in conventional dislocation plasticity and pseudoelastic strain, this effect is called "magnetoacoustic effect".

- It is suggested that the magnetoacoustic effect is not a simple superposition of the external static and stress anisotropy fields but is associated with depinning of trapped magnetic domain walls.

- The suggested interpretation is verified using measurements of the magnetic field hysteresis of the reversible inverse magnetostriction (reversible Villari effect). It is shown that application of ultrasonic oscillations reduces the width of magnetic hysteresis.

5. References

[1] E.K.H. Salje, Multiferroic Domain Boundaries as Active Memory Devices: Trajectories Towards Domain Boundary Engineering, ChemPhysChem 11 (2010) 940-950.

[2] A. Aird, E. K. H. Salje, Journal of Physics: Condensed Matter 10 (1998) L377 – L380; A. Aird, M. C. Domeneghetti, F. Mazzi et al., Journal of Physics: Condensed Matter 10 (1998) L569 – L574.

[3] S. Van Aert, S. Turner, R. Delville, D. Schryvers, G, Van Tendeloo, E.K.H. Salje, Direct observation of ferrielectricity at ferroelastic domain boundaries in CaTiO3 by electron microscopy, Advanced Materials, 24 (2012) 523-7.

[4] E. K. H. Salje, M. Alexe, S. Kustov, M. C. Weber, J. Schiemer, G. F. Nataf, J. Kreisel, Direct observation of polar tweed in $LaAlO_3$, Scientific Reports 6 (2016) 27193.

[5] G. Bertotti, I. Mayergoyz, The science of hysteresis, Eds., Elsevier 2005.

[6] S. Kustov, J. Torrens-Serra, E. K. H. Salje, D. N. Beshers, Re-entrant spin glass transitions: new insights from acoustic absorption by domain walls, Scientific Reports 7 (2017) 16846.

[7] V.F. Coronel, D.N. Beshers, Magnetomechanical damping in iron, Journal of Applied Physics 64 (1984) 2006-2015.

[8] G. Bertotti, Hysteresis in Magnetism, Academic Press, San Diego California, 1998.

[9] A.S. Nowick, B.S. Berry, Magnetoelastic relaxations and hysteresis damping of ferromagnetic materials, Chapter 18 in: Anelastic relaxation in crystalline solids, Academic Press, New York-London, 1972.

[10] J. Degauge, Magnetic Domains, Chapter 6.1 in: Mechanical Spectroscopy Q-1 2001 with applications to materials science, R. Schaller, G. Fantozzi and G. Gremaud, Eds., Trans Tech Publications Ltd., Switzerland, 2001.

[11] S. Kustov, M.-Ll. Corró, V. Kaminskii, A. Saren, A. Sozinov, K. Ullakko, Elastic and anelastic phenomena related to eddy currents in cubic Ni_2MnGa, Scripta Materialia 147 (2018) 69-73.

[12] G.W. Smith, J.R. Birchak, Effect of internal stress distribution on magnetomechanical damping, Journal of Applied Physics 39 (1968) 2311-2316.

[13] G.W. Smith, J. R. Birchak, Internal stress distribution theory of magnetomechanical hysteresis: an extension to include effects of magnetic field and applied stress, Journal of Applied Physics 40 (1969) 5174-5178.

[14] I. Aaltio, A. Sozinov, Y. Ge, K. Ullakko, V.K. Lindroos, S.-P. Hannula, in: S. Hashmi (Ed.), Reference Module in Materials Science and Materials Engineering, Elsevier, Oxford, 2016 1–14.

[15] K. Ullakko, J.K. Huang, C. Kantner, R.C. O'Handley, V.V. Kokorin, Large magnetic-field-induced strains in Ni_2MnGa single crystals, Applied Physics Letters 69 (1996) 1966-1968.

[16] S. Kustov, J. Rosselló, M.-Ll. Corró, V. Kaminskii, K. Sapozhnikov, A. Saren, A. Sozinov and K. Ullakko, Magnetic domain walls and macroscopic magnetization-related elastic and anelastic effects during premartensitic transition in Ni2MnGa, Materials 12 (2019) 376.

[17] C. Salazar Mejía, N.-O. Born, A. Scheimer, C. Felzer, M.A. Carpenter, M. Nicklas, Strain and order parameter in Ni-Mn-Ga Heusler alloys from resonant ultrasonic spectroscopy, Physical Review B 97 (2018) 094410.

[18] L. Straka, A. Soroka, H. Seiner, H. Hänninen, A. Sozinov, Temperature dependence of twinning stress of Type I and Type II twins in 10M modulated Ni-Mn-Ga martensite, Scripta Materialia 67 (2012) 25-28.

[19] S. Kustov, M.-Ll. Corró, V. Kaminskii, A. Saren, A. Sozinov, K. Ullakko, Elastic and anelastic phenomena related to eddy currents in cubic Ni_2MnGa, Scripta Materialia 147 (2018) 69-73 (Supplementary Material 2).

[20] S.P. Venkateswaran, N.T. Nuhfer, M. De Graef, Anti-phase boundaries and magnetic domain structures in Ni_2MnGa-type Heusler alloys, Acta Materialia 55 (2007) 2621-2636.

[21] M. De Graef, M.A. Willard, M.E. McHenry, Y. Zhu, In-situ Lorentz TEM cooling study of magnetic domain configurations in Ni2MnGa, IEEE Transactions on Magnetics 37 (2001) 2663-2665.

[22] W.H. Robinson, A. Edgar, Piezoelectric method of determining mechanical damping at frequencies of 30 to 200 kHz, IEEE Transactions on Sonics and Ultrasonics SU21 (1974) 98-105.

[23] S. Kustov, S. Golyandin, A. Ichino, G. Gremaud, A new design of automated piezoelectric composite oscillator technique, Material Science Engineering A 442 (2006) 532–537.

[24] S. Kustov, F. Masdeu, E. Cesari, Mechanomagnetic spectroscopy of phase transitions in ferromagnetic shape memory alloys, Applied Physics Letters 89 (2006) 061917-3.

[25] S. Kustov, M.L. Corro, E. Cesari, Mechanomagnetic spectroscopy of ferromagnetic shape memory alloys, Materials Science and Engineering A 521–522 (2009) 194–200.

[26] R. H. Chambers and R. Smoluchowski, Time-dependent internal friction in aluminium and magnesium single crystals, Physical Review 117 (1960) 725-731.

[27] Bozorth, R.M. Chapter 13 in: Ferromagnetism;Wiley-IEEE Press: Hoboken, NJ, USA, 2003, pp. 595–712.

[28] D. Gignoux, M. Schlenker, É.D.T. de Lacheisserie, Chapter 12 in: Magnetism. Fundamentals; Springer: New York, NY, USA, 2005;, pp. 351–397.

[29] https://en.wikipedia.org/wiki/Earth´s_magnetic_field

[30] M.-L. Corró, Y.I. Chumliakov, J. Torrens-Serra, S. Kustov, Peculiarities of magnetoelastic coupling in $Ni_{51.5}Fe_{21.5}Ga_{27}$ single crystals, Journal of Physics D: Applied Physics 46 (2013) 375002 (7pp).

[31] D. Damjanovic, Hysteresis in piezoelectric and ferroelectric materials, Chapter 4 in: The science of hysteresis, G. Bertotti and I. Mayergoyz, Eds., Elsevier, 2005.

[32] F. Blaha and B. Langenecker, Plastizitätsuntersuchungen von metallkristallen in ultraschallfeld, Acta Metallurgica 7 (1959) 93-100.

[33] A.B. Lebedev, Internal friction in quasi-static crystal deformation, Physics of the solid state (Fizika Tverdogo Tela) 35 (1993) 2305-2341.

[34] K.V. Sapozhnikov, V.V. Vetrov, S.A. Pulnev, S.B. Kustov, Acousto-pseudoelastic effect and internal friction during stress-induced martensitic transformation in Cu-Al-Ni single crystals, Scripta Materialia 34 (1996) 1543-1548.

[35] T. Sakon, Y. Hayashi, D. Li, F. Honda, G. Oomi, Y. Narumi, M. Hagiwara, T. Kanomata, T. Eto, Forced magnetostrictions and magnetizations of $Ni_{2+x}MnGa_{1-x}$ at its Curie temperature, Materials 11 (2018) 2115.